TFE Terpolymers: Once Promising -Are There Still Perspectives in the 21st Century: Synthesis, Characterization, and Properties-Part I

Salim Ok, Martin Steinhart, Ulrich Scheler, Bruno Améduri

TFE Terpolymers: Once Promising - Are There Still Perspectives in the 21st Century: Synthesis, Characterization, and Properties-Part I

Salim Ok[a,*], *Martin Steinhart*[b], *Ulrich Scheler*[c], *Bruno Améduri*[d,*]

[a,#] Petroleum Research Center, Kuwait Institute for Scientific Research, P.O. box 24885 Safat, 13109, Kuwait

[b] School of Biology and Chemistry and CellNanOs, Universität Osnabrück, Barbarastr. 7, 49069 Osnabrück, Germany

[c] Leibniz-Institut für Polymerforschung Dresden e.V. Dresden, Hohe Strasse 6, D-01069 Dresden, Germany

[d]Institut Charles Gerhardt, Univ. Montpellier, CNRS, ENSCM, Montpellier, France

*Corresponding authors, E-mail: sok@uos.de, bruno.ameduri@enscm.fr

Polytetrafluoroethylene (PTFE) exhibits outstanding properties such as high-temperature stability, low surface tension, and chemical resistance against most solvents, strong acids and bases. However, these traits make it challenging to subject PTFE to standard polymer processing procedures, such as thermoforming and hot incremental forming. While polymer processing at temperatures above the melting point of PTFE is already demanding, the typically large molar mass of PTFE results in extremely high melt viscosities, complicating the processing of PTFE. In addition, PTFE tends to decompose at temperatures close to its melting point. Therefore, fluoropolymers obtained by copolymerizing TFE with various co-monomers were studied as alternatives to PTFE (e.g. fluorinated ethylene-propylene (FEP)), combining its advantages with better processability. TFE terpolymers have emerged as desirable PTFE alternatives. This review provides an overview of the synthesis with various comonomers and microstructural analysis of PTFE terpolymers and the relationships between the microstructures of TFE terpolymers and their properties.

Keywords. TFE-based terpolymers, synthesis, characterization

Abbreviations List. DBU: 1,8-Diazabicyclo[5.4.0]undec-7-ene. NFH: 3,3,4,4,5,5,6,6,6-nonafluorohexene. TFP: 3,3,3-trifluoropropene. FA3: 4,5,5-trifluoro-4-penten-1-ol. AA: acrylic acid. AFM: atomic force microscopy. ATR: attenuated total reflection. ATR-FTIR: attenuated total reflection-Fourier transform infrared. BZ: Belousov-Zhabotinsky. CB: carbon black. CNT: carbon nanotube. CSI: Coherence scanning interferometry. CFU: colony-forming unit. Cloisite NA: commercial non-modified montmorillonite. FC-2175: copolymer of VDF and HFP. CuAAC: copper(I)-catalyzed azide-alkyne cyclo-addition. T_c: critical temperature. COC: cyclic olefin copolymer. DAC: diamond anvil cell. DSC: differential scanning calorimetry. DIPS: diffusion-induced phase separation. DMF: N, N-dimethylformamide. DMAc: dimethylacetamide. DC: direct current. DBR: Distributed Bragg Reflector. DFB: Distributed FeedBack. DMA: dynamic mechanical analysis. EBMA: electret-based mechanical antenna. EAP: electron accumulation polymer. EPR: electron paramagnetic resonance. E_b: elongation percent at break. ESD: Electrostatic discharge. E: ethylene. EO: ethylene-octene. EVE: ethyl vinyl ether. EOS: equation of state. FEP: fluorinated ethylene-propylene. FP: fluoropolymer. FTO: fluorine-doped tin oxide. NB-F-OH: fluoroalcohol-substituted norbornene. ^{19}F: Fluorine-19. FT-IR: Fourier transform-infra red. GDVN: Gas dynamic virtual nozzle. T_g: glass transition temperature. GVE: glycidyl vinyl ether. gCOSY: gradient correlation spectroscopy. gDQCOSY: gradient double quantum correlation spectroscopy. gHSQC: gradient heteronuclear single quantum correlation. GNP: graphene nanoplatelets. HFPO: hexafluoropropylene oxide. DIAK 1: hexamethylenediamine carbamate. HDPE: high-density polyethylene. HF: hydrofluoric acid. H_2O_2: hydrogen peroxide. IEC: Ion Exchange Capacity. Pb: Lead. LCB: long-chain branching. G'': loss modulus. tan δ: loss tangent. MAS: Magic Angle Spinning. MgB_2: magnesium diboride. ΔH_m: melt enthalpy. T_m: melting temperature. MEK: methyl ethyl ketone. MIBK: methyl isobutyl ketone. NMP: N-methyl pyrrolidone. MCNT: modified surface carbon nanotube. M_w: molar mass. MMT: montmorillonite. MALLS: multiangle laser light scattering. MWNT: multi-walled nanotube. MWCNT: multi-walled carbon nanotube. NOA: Norland optical adhesive. M_n: number average molar mass. N-vinylpyrrolidone: NVP. M_wD: molar mass distribution. NBVE: n-butyl vinyl ether. 1D: one-dimensional. O-MMT: organically modified montmorillonite. M_w/M_n (PDI): polydispersity index. NMR: nuclear magnetic

resonance. NOESY: nuclear Overhauser effect spectroscopy. P_c: critical pressure. PFAS: per- and polyfluoroalkyl substances. PAVE: perfluoroalkyl vinyl ether. PFBE: perfluorobutylethylene. PDCPD: perfluorodicyclopentadiene. PMVE: perfluoromethyl vinyl ether. PPVE: perfluoro(propyl vinyl). PCTFE: polychlorotrifluoroethylene. Poly (CTFE-*co*-VDF): poly (chlorotrifluoroethylene-*co*-vinylidene fluoride). PDMSMA: poly(dimethyl siloxane) methyl acrylate-terminated. PE: poly (ethylene). EO: poly (ethylene octene). PC: polycarbonate. PLC: Polymers of low concern. PMMA: poly (methyl methacrylate). PS: polystyrene. SAN25: polystyrene 75 wt% and acrylonitrile 25 wt%. PTFE: poly(tetrafluoroethylene). PVDF: poly(vinylidene fluoride). PV: pressure-volume. KOH: potassium hydroxide. P: propylene. PVE: propyl vinyl ether. R_g: radius of gyration. R6G: rhodamine 6G. SECM: scanning electrochemical microscopy. SEC: size exclusion chromatography. SAXS: small-angle X-ray scattering. SWCNT: single wall carbon nanotubes. E': storage modulus. SubCW: subcritical water. sc CO_2: supercritical carbon dioxide. SEM: scanning electron microscopy. SECM: scanning electrochemical microscopy. T_b: tensile strength. THF: tetrahydrofuran. TIPS: thermally induced phase separation. TGA: thermo-gravimetric analysis. *t*BuAc: *tert*-butyl acrylate. THF: tetrahydrofuran. THV: Terpolymer of Tetrafluoroethylene (**T**FE), Hexafluoropropylene (**H**FP), and Vinylidene fluoride (**V**DF). MXene: $Ti_3C_2T_x$. TTS: time-temperature superposition. TOCSY: total correlation spectroscopy. TEM: transmission electron microscopy. TENGS: triboelectric nanogenerators. CF_3NO: trifluoronitrosomethane. 2D: two-dimensional. UV: ultraviolet. UTM: universal testing machine. VAc: vinyl acetate. VA: vinyl alcohol. M_w: weight-average molar mass. WAXD: Wide-angle X-ray diffraction. WAXS: wide-angle X-ray scattering. XRD: X-ray diffraction. XPS: X-ray photoelectron spectroscopy. ε: branching factor. η^*: complex viscosity. g_η: contraction factor. χ_c: crystallinity. K: dielectric constant. η: intrinsic viscosity.

Table of Content

1. Introduction: Short History

Since the unintentional discovery of poly(tetrafluoroethylene) (PTFE) in 1938, marketed as Teflon® in 1941,[1] fluorine-containing polymers have attracted significance in science and technology.[2] Fluoropolymers (FPs) are niche macromolecules of high molar mass (M_w) polymers (up to several million g/mol) with fluorine atoms directly bonded to the backbone having carbon only.[3-4] As perfluoropolymers and semi-fluorinated polymers,[5] FPs are classified from thermoplastics, elastomers, and plastomers to thermoplastic elastomers.[6] Furthermore, among per- and polyfluoroalkyl substances (PFAS), FPs represent a unique class because they satisfy the most accepted polymer hazard evaluation parameters to be defined as polymers of low concern (PLC). Indeed, they fulfill the 13 PLC criteria in terms of physicochemical characteristics, such as M_w, charges, no residual monomers, no solubility in water, or no leachables.[4] Their high molar mass, chemical inertness, and insolubility make them also of low concern from the perspectives of human health and environmental issues.[4]

The unique fluorinated polymers can be either semi-crystalline or amorphous.[7] The carbon-fluorine bond is the strongest bond between a carbon atom and another one. This uniqueness gives outstanding and beneficial characteristics and results in the extraordinary functioning of FPs.[8] These halogenated polymers exhibit excellent chemical stability even at elevated temperatures, slow aging, excellent weather resistance, low friction coefficients and surface tensions, low dielectric constants, and low moisture uptake.[5, 7, 9] Hence, FPs have been employed in various chemical, electronic, construction, architectural, and automotive applications.[5] FPs have been utilized as ultraviolet (UV) and graffiti-resistant paint materials, seals, gaskets, O-rings, high-quality membranes with excellent separation performance, core and cladding of optical fibers, biomedical materials[10-12] and special coatings for old monuments.[7]

The drawback of PTFE is its complicated processing. Because of its high melting temperature of 327 °C, close to that of its degradation, and its typically high melt viscosity,[5] common thermoforming applied for the processing of thermoplastics is not viable. The low solubility in common organic solvents[7, 13] also prevents the application

of solution-based processing methods, such as spin coating for generating thin film, castings coating, and fiber fabrics.

The hurdles in processing or dissolving PTFE motivated researchers to synthesize and develop copolymers and terpolymers of tetrafluoroethylene (TFE) with other monomers, including vinylidene fluoride (VDF) or hexafluoropropylene (HFP) or even both monomers, to improve processing and characterization in solution. The introduction of side groups, such as $–CF_3$ by incorporation of HFP, produces disorder in the macromolecules; this disorder reduces the crystallinity of the homopolymer and may even suppress crystallization.[7, 13] Insertion of VDF monomers has a similar effect in reducing creep[14] and reduces the crystallinity effectively. By varying the monomers, the number of TFE-based terpolymers has been increased.[15]

Table 1 lists the TFE-based terpolymers covered herein. The dispersity of the literature on TFE-based terpolymers makes it essential to assemble the know-how on these fluorinated PLCs from human and environmental health concerns. This part of the two review articles focuses on the synthesis, microstructural assignments, and properties of TFE terpolymers, while the second one deals with the applications. Hence, the present review article aims to fill the information gap on TFE-based terpolymers.

Table 1. Various modified TFE terpolymers.

Number	Name of Polymer	Reference
1	TFE-HFPO-CF_2=$CFOCF_3$	[15]
2	TFE-perfluoro-(2-methylene-4-methyl-1,3-dioxolane)-perfluoroethylenebis (divinyl ether)	[16]
3	TFE--CH(OR)-CH_2-CH(O-CH_2-CH_2-X)-CH_2-	[17]
4	TFE-(CF_3NO)-($CN_3O_2CCFClNO$)	[18]
5	TFE-PMVE-PDCPD	[19]
6	TFE-(CF_3NO)-(difluoromaleic anhydride)	[20]

7	TFE-HFP-PVE	[21]
8	TFE-HFP-EVE	[21]
9	TFE-P-GVE	[22]
10	TFE-HFP-AA	[23]
11	TFE-P-FA3	[24]
12	TFE-VAc-VA	[25]
13	TFE-VAc-PDMSMA	[26]
14	TFE-*t*BuAc-NB-F-OH	[27]
15	TFE-HFP-VDF	[28]
16	TFE-P-VDF	[29]
17	TFE-P-NBVE	[30]
18	TFE-P-TFP	[31]
19	E-TFE-HFP	[32]
20	E-TFE-NFH	[32]
21	E-TFE-nonafluoro-1-hexene	[33]
22	E-TFE-HFP	[33]
23	TFE-PAVE-PFBE	[34]
24	TFE-VDF-PMVE	[34]
25	TFE-E-PMVE	[34]
26	TFE-PMVE-8CNVE	[34]
27	TFE-MOVE-VDF	[34]
28	Viton, THV elastomer	[35]
29	TFE-PPVE-dimethyl (3-trifluoroethenoxyhexafluoropropyl)phosphonate	[36]
30	TFE-PPVE-M_x M_1: (3-trifluoroethenoxyhexafluoropropyl) phosphonate M_2: diethyl (2-trifluoroethenoxytetrafluoroethyl) phosphonate M_3: diethyl (trifluoroethenoxy-4-trifluoromethyl-3-oxaperfluoropentyl)phosphonate	[37]

TFE: tetrafluoroethylene, PMVE: perfluoromethyl vinyl ether, PDCPD: perfluorodicyclopentadiene, HFP: hexafluoropropylene, PPVE: perfluoro(propyl vinyl) ether; PVE: propyl vinyl ether, EVE: ethyl vinyl ether, P: propylene, GVE: glycidyl vinyl ether, AA: acrylic acid, FA3: 4,5,5-trifluoro-4-penten-1-ol, VAc: vinyl acetate, VA: vinyl alcohol, PDMSMA: poly(dimethyl siloxane) methyl acrylate-terminated, *t*BuAc: *tert*-butyl acrylate, NB-F-OH: fluoro alcohol-substituted norbornene, HFPO: hexafluoropropylene oxide, VDF: vinylidene fluoride, NBVE: n-butyl vinyl ether, TFP: 3,3,3-trifluoropropene, E: Ethylene, NFH: 3,3,4,4,5,5,6,6,6-nonafluorohexene. PFBE: perfluorobutyl ethylene. PAVE: perfluoroalkyl vinyl ether. MOVE: CF_3-(O-CF_2-O)n-CF=CF_2. CNVE: CF_2=CFOCF_2CF(CF_3)OCF_2CF_2CN

2. Synthesis, Microstructural Assignments, and Average Molar Mass Determination

2.1 Synthesis

Selman and Squire[16] terpolymerized TFE with two monomers of perfluoro-(2-methylene-4-methyl-1,3-dioxolane) and perfluoroethylene-bis(divinyl ether) (Figure 1).[15] The divinyl ether feed fraction was 0.5 wt% and that polymerization yielded a transparent film cast cross-linkable upon heating between 100 and 340 ^{o}C.

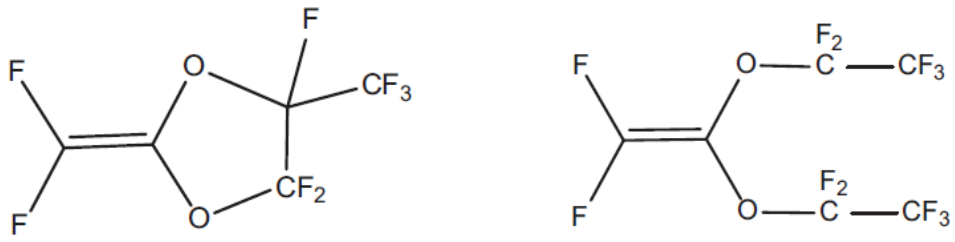

Figure 1. Chemical structures of the two monomers, perfluoro-(2-methylene-4-methyl-1,3-dioxolane) (left) and perfluoroethylene bis(divinyl ether) (right), involved with the terpolymerization with TFE.[15]

Pattison[17] attempted synthesizing a terpolymer based on TFE (45 to 55 mol.%), -(OR)-CH-CH_2 (54.8 to 35 mol.%), and approximately 0.2 to 10 mol.% of

-CH-CH_2- base unit.
|
O-CH_2-CH_2-X

In -(OR)-CH-CH_2, R is a saturated aliphatic hydrocarbon radical with 1 to 18 carbons or a radical of R'-O-CH_2-CH_2- with a potential that R' is a saturated aliphatic hydrocarbon radical with 1 to 4 carbons. In the monomer with the lowest percentage, X is a halogen radical such as iodine, chlorine, and bromine, the hydroxyl group (-OH) or a radical of the chemical -NH-C(=O)-Y where Y is either hydrogen or a saturated aliphatic hydrocarbon radical with 1 to 8 carbons.

Oliver and Stump[18] synthesized a series of fluorinated copolymers and terpolymers. Both terpolymers are based on TFE, CF_3NO (trifluoronitrosomethane), and $CN_3O_2CCFClNO$ monomers: both monomers surprisingly open the π bond in the N=O group. The relative molar ratios were 50, 40, and 10 for TFE, CF_3NO, $CN_3O_2CCF_2NO$, or $CH_3O_2CCFClNO$, respectively. The reactions were conducted for 48 hours at -35 ^oC to avoid potential explosions.

Harris[19] prepared a series of hexafluorocyclopentadiene and perfluorodicyclopentadiene (PDCPD)-based copolymers and terpolymers, such as terpolymer of PDCPD/HFP/VDF. The interest of the current article is on the terpolymer of TFE, perfluoromethyl vinyl ether (PMVE), and PDCPD [poly(TFE-*ter*-PMVE-*ter*-PDCPD) terpolymer]. The FTIR spectra displayed absorption bands at 1760 and 995 cm^{-1} assigned to PDCPC as indicative bands of the successful synthesis of the final product. The synthesis was started with perfluorodicyclopentadiene, and the yield was nearly 49%.

TFE and PMVE-based terpolymers were also synthesized using additional comonomers such as methyl perfluoro-5-oxa-6-heptenoate, and perfluoro-6-oxa-7-octenoyl fluoride, perfluoro-5-oxa-6-heptene-nitrile, and perfluoro-6-oxa-7-octene.[38] The polymerization occurred in an aqueous medium containing phosphate and ammonium perfluorooctanoate as surfactants. The yield of the solid poly(TFE-*ter*-PMVE-*ter*-methyl perfluoro-6-oxa-7-octenoate) terpolymer after 5 hour-reaction was 85%, that of poly(TFE-*ter*-PMVE-*ter*-perfluoro-5-oxa-6-heptene nitrile) one was 16%, while that of poly(TFE-*ter*-PMVE-*ter*-perfluoro-6-oxa-7-octenenitrile) terpolymer was

43%. The produced TFE and PMVE-based terpolymers were vulcanizable and demonstrated suitable tensile strengths and resistances to environmental attacks.

Jones[20] successfully prepared a terpolymer of TFE, perfluoronitrosomethane, and difluoromaleic anhydride (Figure 2) initiated by an organic peroxide at -20 °C for 64 hours, during which the autogenous pressure decreased from 1.72 MPa to 0.12 MPa. The resulting TFE-based terpolymer exhibited outstanding chemical and thermal properties.

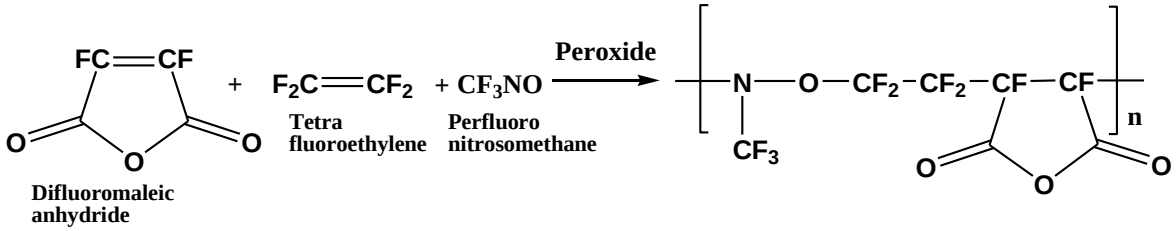

Figure 2. Terpolymer of TFE, perfluoronitrosomethane, and difluoromaleic anhydride where n is an integer value between 45 and 2800.[20]

Carlson et al.[21] synthesized TFE-HFP-propyl vinyl ether (PVE) and TFE-HFP-ethyl vinyl ether (EVE)-based terpolymers (considering TFE and HFP as accepting monomers while the vinyl ethers are donating ones), either in an aqueous or non-aqueous-medium, either in chlorofluorohydroalkanes as the solvents. Both these modified PTFE terpolymers were melt-processible compared to PTFE while having satisfactory properties of stability and tensile strength at elevated temperatures, low flammability, anti-stick, and low friction. Poly(TFE-*co*-HFP) copolymers (FEP) demonstrated melting temperature (T_m) approximately 60 ^oC lower than that of PTFE with a *quasi*-similar thermal stability. Both poly(TFE-*ter*-HFP-*ter*-PVE) and poly(TFE-*ter*-HFP-*ter*-EVE) terpolymers displayed better temperature strength than that of FEP because both these terpolymers exhibited T_m of only 20 to 50 ^oC lower than that of PTFE.

Eguchi[22] focused on using cross-linked poly(TFE-*ter*-P-*ter*-GVE) terpolymer (where P and GVE stand for propylene and glycidyl vinyl ether, respectively) to the topmost layer of a rubber stopper. Hence, a cross-linked film was generated by applying heat rather than utilizing cross-linking agents such as peroxides or amines. The rubber stopper's cross-linked fluorinated rubber exhibited excellent adhesiveness and a good

sliding characteristic. The cross-linked fluorinated rubber exhibited excellent resistance against heat, chemicals, and cold.

In the early 1990s, Kostov and Atanasov[23] demonstrated peroxide-induced terpolymerization of TFE with HFP and acrylic acid (AA) as a function of monomer molar ratios, reaction duration, pressure, and the initiator concentration to obtain FPs with ion exchange capacity (IEC) up to 0.8 meq/g. The desired goal was confirmed by Fourier Transform Infrared (FTIR) spectroscopy and the polymers' temperature and phase characteristics. HFP insertion was chosen to lower the T_m and crystallization temperature (T_c) of the polymers to process them. The increase in AA mol% by keeping HFP mol% constant in the synthesis of poly(TFE-*ter*-HFP-*ter*-AA) does not influence T_m and T_c significantly at lower concentrations. The IEC of such terpolymers was changed by the initiator concentration and the mole ratio of the monomers. The terpolymers with relatively good IEC were in the initial monomer mixture above 40 mol% AA fractions.

The same group[39] sulfonated poly(TFE-*ter*-HFP-*ter*-AA) terpolymers with 20 wt% sulfur trioxide in 1,2-dichloroethane at 273 K, and the terpolymer to sulfonating agent ratio was 1/2. Upon sulfonating these terpolymers, the polymers carried sulfo- and carboxyl groups, and their IEC turned out to be 1.75 meq/g, while the degree of sulfonation reached values up to 94%. These sulfonated terpolymers displayed two T_m and T_c values. By means of X-ray diffraction diagrams, the microcrystallite dimension of the sulfonated poly(TFE-*ter*-HFP-*ter*-AA) terpolymer was 540 Å, higher than 401 Å for the parent non-sulfonated terpolymer.

Ameduri et al.[24] revealed the radical emulsion terpolymerization of TFE with P and 4,5,5-trifluoro-4-penten-1-ol (FA3) having hydroxy side groups. The existence of the FA3 monomer lowered the terpolymerization rate compared to the copolymerization of TFE with P. An approximately equimolar ratio between TFE and P units was revealed, while the FA3 was found between TFE and P monomers. The T_g of poly(TFE-*co*-P) based copolymer was lowered from nearly 0 to +5 $^{\circ}$C (i.e., almost -2 and -4 $^{\circ}$C). The thermal composition behavior also demonstrated two steps about the FA3 content. The addition of FA3 monomer into poly(TFE-*co*-P) resulted in a lower M_w and a broader polydispersity index (PDI) for poly(TFE-*ter*-P-*ter*-FA3) than those of poly(TFE-*co*-P).

In a similar study, Kostov et al.[40] synthesized a terpolymer based on TFE and

4,5,5-trifluoro-4-ene pentyl acetate (FAc) monomers initiated by *tert*-butyl peroxy pivalate. ^{1}H and ^{19}F NMR spectroscopy confirmed the reaction, the signals centered at -118 and -120 ppm being assigned to CF_2 in TFE.

The beginning of the current millennium witnessed contributions to the synthesis of novel TFE terpolymers. One of the interesting TFE terpolymers was obtained from the copolymerization of TFE and vinyl acetate (VAc) in supercritical (sc) CO_2 followed by the hydrolysis of VAc into vinyl alcohol (VA) in ethanol, water, and sulfuric acid mixture.[25] In the final stage, sodium bicarbonate was added to the reaction medium. The hydrolysis degree was higher than 80%, and there was only a slight decrease in the molar mass of the terpolymer after the hydrolysis reaction, indicating the loss of acetic acid from VAc.

The same authors[26] also synthesized a series of poly(TFE-*ter*-VAc-*ter*-poly(dimethylsiloxane) methacrylate) terpolymers in sc CO_2 (Figure 3).[26]

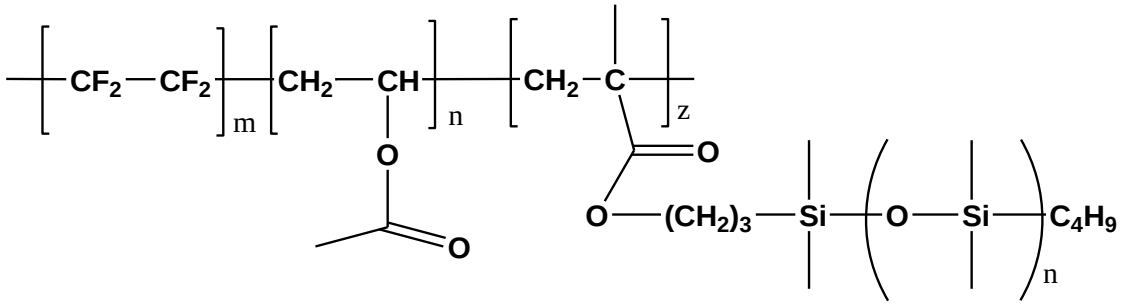

Figure 3. Chemical structure of poly(TFE-*ter*-VAc-*ter*-PDMSMA) terpolymer adapted from Baradie and Shoichet.[26]

The synthesized terpolymers demonstrated good thermal stability, hydrophobicity, and elastomeric features. VAc was introduced into the reaction medium to favor a *termonomer-induced polymerization* because the gap in TFE and PDMSMA reactivity ratios prevented copolymerization. The differential scanning calorimetry (DSC) results revealed a microphase separation for poly(TFE-*co*-VAc) and P(PDMSMA) domains, independent of terpolymer compositions. The terpolymers with a TFE content higher than 55 mol% had additional semicrystalline domains. These peculiar terpolymers were cross-

linked according to a procedure developed by Jacks for generating a low-compression set fluoroelastomer foam.[41] Upon 14 days of continuous heating at 200 °C in air, the crosslinked terpolymer had only 5% mass loss. When the molar mass of the linear terpolymer, fluorocarbon composition, and curing time were increased, the elastic modulus of the resulting material also increased. The uncross-linked and cross-linked terpolymers exhibited hydrophobicity compared to those of TFE and VAc-based copolymers. The orientation of the pendant PDMS groups at the air surface was explained by greater mobility and lower surface tension than those of $-CF_2$ groups of TFE monomers. These terpolymers were involved in coating applications.

In addition, Feiring et al.[27] designed a terpolymer consisting of TFE, *tert*-butyl acrylate (*t*-BuAc), and a fluoro alcohol-substituted norbornene (NB-F-OH) (Figure 4) for photoresist applications.

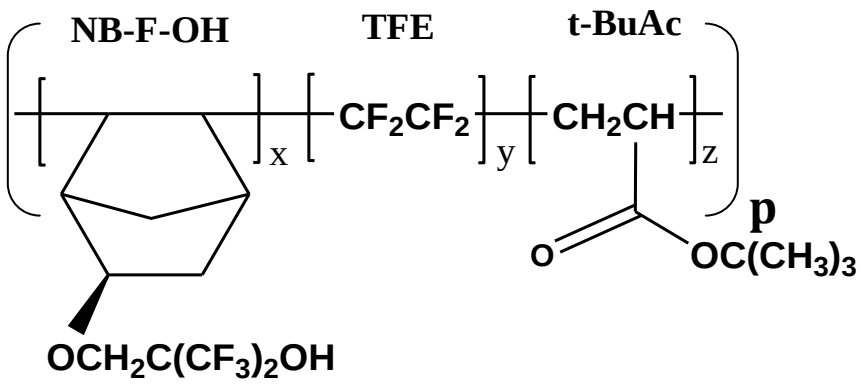

Figure 4. Chemical structure of poly(NB-F-OH-*ter*-TFE-*ter*-*t*-BuAc) terpolymer.[27]

Synthesizing this TFE terpolymer aimed at developing a transparent FP as a resisting semiconductor at 157 nm. A polymer binder with transparency at the imaging wavelength is the most critical component of a modern photo-resisting system. In this regard, the role of fluorine induced i) the absorption spectrum of materials at short wavelengths and ii) an enhanced acidity of different functional groups.

Other original TFE terpolymers were also synthesized.[15] A specific non-conjugated diene, CF_2=CF-O-$(CF_2)_3$-CF=CF_2, as the well-known precursor of the cyclic transparent optical polymer (CYTOP® manufactured by AGC Company) was

terpolymerized at 0.01-1.00 mol% with TFE and PMVE, yielding a fluoroelastomer without any T_m. Still, the T_g is usually below 0 ^oC and might reach up to 25 ^oC depending on the composition of the terpolymer.[42-43]

Among the modified TFE terpolymers, one of the most important FPs is the terpolymer based on **T**FE, **H**FP, and **V**DF (THV) (Figure 5).

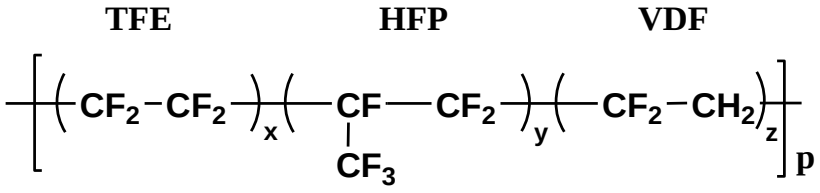

Figure 5. Monomeric units of THV. TFE, HFP, and VDF stand for tetrafluoroethylene, hexafluoropropylene, and vinylidene fluoride, respectively.[44]

The THV fluoroelastomer is marketed by 3M company under the Fluorel® FT2350 or FE5830QD tradenames, while Chemours (formerly Dupont) also commercializes elastomeric THV under the Viton® B or Viton® F trademarks.[45] Figure 6 exhibits how THV elastomer or thermoplastic are obtained depending on the comonomer composition.[46] The fluorothermoplastic version of THV is produced by Dyneon.[28]

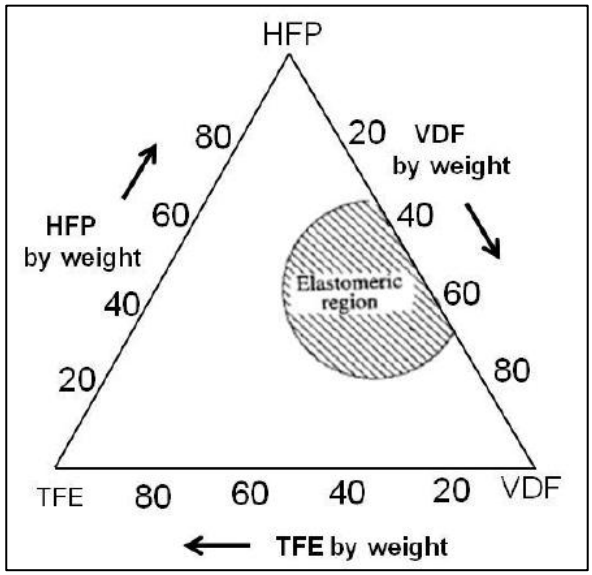

Figure 6. Semi-crystalline or amorphous regions according to the compositions of VDF, HFP, and TFE (THV terpolymer) (reproduced with permission from Wiley).[46]

An important parameter to be highlighted in finding suitable applications for polymers is the T_g, representing a thermal point where remarkable changes in polymer properties happen.[47-48] Bonardelli et al.[47] synthesized poly(VDF-*co*-HFP) and poly(TFE-*ter*-HFP-*ter*-VDF) co/terpolymer by semi-continuous emulsion polymerization. In the terpolymer, as the TFE percentage decreases, T_g decreases. Moreover, the T_g's dependence on the composition was not linear; rather, the sequence orders influenced the T_g values of both the copolymer and terpolymer. The highest and the lowest recorded T_g values were 271.5 K and 252.0 K, respectively.[47] The same group continued their efforts on the sequence distribution of both VDF fluoroelastomers with deep ^{19}F NMR spectroscopic characterizations with correlation with some properties.[49] In addition, as expected, as the VDF content increased, the T_g decreased.[49-50]

Taguet et al. reviewed a linear correlation between the TFE percentage and T_g values determined for the poly(TFE-*ter*-HFP-*ter*-VDF) terpolymers.[51] Besides, the terpolymers were cross-linked by inorganic bases such as $Ca(OH)_2$ and telechelic diamines or bisphenol AF. Utilization of base formed double bonds by VDF dehydrofluorination in poly(VDF-*ter*-HFP-*ter*-TFE) terpolymers.[52] At the same time, cross-linking was completed by nucleophilic addition of diamines or bisphenol AF onto the double bonds. Cross-linking relied on the VDF fraction rather than the HFP-VDF-HFP triad. The effect of the sequences on T_g was explained by i) upon increasing the VDF fraction, the contribution of hydrogen bonding to T_g was lowered, and ii) the influence of HFP onto T_g was less expected because the polymer chains were free of the steric strain imposed by the interactions between $-CF_3$ groups of HFP on adjacent carbon atoms of HFP units. This study exhibits correlating microstructural sequence orders to the properties of fluorinated terpolymers.[51]

In addition to T_g and T_m values, continuous use and processing temperatures are crucial in utilizing FPs. Compared to the typical continuous use temperature and processing temperature of PTFE as 260 ^oC and 380 ^oC, respectively, THV has a range of

70-130 ^{o}C and 171-310 ^{o}C for the exact utilization and processing temperatures,[53] above which FPs might start a thermal degradation.

In evaluating the synthetic pathways in the synthesis of THV via free radical polymerization, the existence of closer structures to those derived from the TFE homopolymerization is anticipated. Depending on the comonomer composition, the terpolymer is expected to have primarily randomly distributed TFE, VDF, and HFP unit sequence orders. For the given conditions of the copolymerization procedure, HFP monomer is known not to homopolymerize.[49, 54-55] For the non-symmetrical VDF and HFP units, the radicals formed at the initial stages of the polymerization can attach to either end of the monomer. A possible attachment to the **C**F(CF_3) carbon of HFP and CF_2 carbon in VDF is less preferable due to the steric and electronic factors. Hence, the regular/inverse addition to VDF or HFP monomer could form different end groups, as Twum et al. comprehensively detailed the NMR clarification of such copolymers.[56] Along the polymerization, the insertion of a monomer unit onto a growing macromolecular radical occurs in a preferred direction.[57-58]

Kaspar et al.[59] developed some new THV grades by solution and suspension polymerizations. In one form of synthesizing fluorothermoplastics, a reactive olefin bearing a bromine or iodine atom was utilized as a cure site monomer. The olefin has the following general formula: $X_2C=CXZ$, where each X could be the same or differ from each other and represents either H, F, Cl, Br, and I. Z refers to H, F, Cl, Br, I, a perfluoroalkyl group, a perfluoroalkoxy group, or a perfluoropolyether group. The thermoplastics invented by Kaspar et al. have long chain branchings (LCBs),[59] thought to be due to the abstraction of the bromine or iodine atom from the modifier once it is polymerized into the backbone of the FP. The generated radical during the polymerization might result in further polymerization, leading to the branch on the backbone as a polymer chain. The serious effects of these LCBs on the properties of FPs were highlighted by rheological studies.[59]

Another subclass of TFE terpolymers contains phosphorus. Yamabe et al.[36] pioneered the synthesis of copolymers of TFE and dimethyl (3-trifluoroetheneoxyhexafluoropropyl)phosphonate (M_0) (Figure 7) and recognized the poor flexibility of the yielded copolymer films.

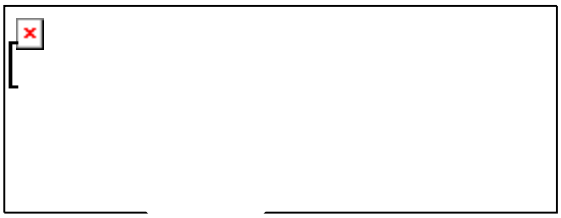

Figure 7. Copolymer of tetrafluoroethylene and dimethyl (3-trifluoroethenoxyhexafluoropropyl)phosphonate.[36]

Therefore, perfluoro(propyl vinyl ether) (PPVE) was utilized to synthesize a TFE-based terpolymer. Involving PPVE as the third comonomer resulted in an enhancement in elongation (110%) compared to that of the copolymer of TFE and M_0 (30%) for the same applied tensile strength (2.1 kg/cm^2), proving the increase in the flexibility of the terpolymer. The terpolymer and the copolymer demonstrated the same thermal decomposition and melt flow index. They were prepared to compete with Nafion® membranes for fuel cell applications after the hydrolysis of dialkyl phosphonate units into phosphonic acid.

In a similar objective, Kotov et al.[37] terpolymerized monomers M1, M2, and M3 (Figure 8 and Table 1) with TFE and PPVE in emulsion, with a yield reaching up to 59%. The thermal decomposition of the polymers was ranging between 240 and 310 ^{o}C because of the loss of ethyl groups in the diethyl phosphate function. Hydrolysis of the phosphonate group into phosphonic acid was monitored by hot pressing, and the final processing of the terpolymer led to films, the thickness of which ranged between 0.10 and 0.13 mm.

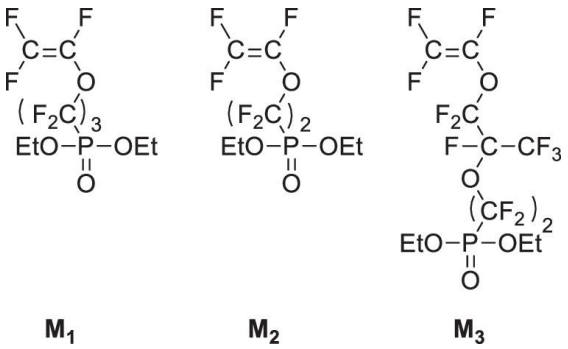

Figure 8. Structures of (3-trifluoroethenoxyhexafluoropropyl) phosphonate (M_1), diethyl (2-trifluoroethenoxytetrafluoroethyl) phosphonate (M_2), and diethyl (trifluoroethenoxy-4-trifluoromethyl-3-oxaperfluoropentyl)phosphonate (M_3) as comonomers of TFE.[37]

2.2 Microstructural Assignments

Six kinds of Poly(TFE-*ter*-P-*ter*-VDF) terpolymers with two different molar percentages of 48:49:3 and 38:29:33 for TFE:P:VDF were synthesized.[29] The comparison of unsaturated bond normalized to poly(TFE-*ter*-P-*ter*-VDF) terpolymer with 33 mol% of VDF after wet treatment indicated identical results. While the wet treatment resulted in a more significant fraction of unsaturation, the probe with a higher VDF percentage had a higher introduced unsaturation. There could be a trace of unsaturation in the as-polymerized sample, and for the probe with a small percentage of VDF, the wet and dry treatments had the same influence. Note that the introduction of the unsaturated bond as vulcanization sites *via* the reaction of the aqueous dispersion of terpolymer in alkali solution by phase transfer catalyst is considered as a wet treatment. On the other hand, that of the saturated terpolymer in the solid state by quaternary ammonium molecules for Bisphenol-AF vulcanization yields better thermal and chemical longevity due to no excess introduction of the unsaturated bond, defined as a dry treatment.

Various research groups contributed to clarifying the microstructures of THV by ^{19}F NMR spectroscopy in solution[60] and in solid-state,[61] at high temperatures in the melt.[62] All the ^{19}F NMR signals assigned to the expected signals in the poly(VDF-*co*-TFE) copolymer were observed in the NMR spectrum of THV.[60] HFP units were mainly adjacent to VDF units. Indeed, the VDF-HFP-VDF, HFP-VDF-HFP, and VDF-VDF-

HFP triads were evidenced while new HFP-VDF-TFE-VDF-TFE and HFP-VDF-TFE-VDF-VDF pentads (where TFE units were next to VDF units rather than HFP) were highlighted.[60]

The monomer moieties in poly(TFE-*ter*-HFP-*ter*-VDF) terpolymers synthesized by Pianca et al.[49] displayed randomly distributed microstructures. The growing radical with the most often encountered head-to-tail propagation and head-to-head and tail-to-tail propagations in lower percentages usually reacts onto the monomer. ^{19}F NMR spectroscopy also revealed the following sequence order: VDF-HFP-VDF-HFP-VDF, TFE-HFP-VDF-HFP-VDF, HFP-VDF-HFP-VDF-HFP-TFE, TFE-HFP-VDF-TFE.

As quantitative analysis of ^{19}F magic angle spinning (MAS) NMR spectra illustrates, FLS 2690 consists of 58 mol % VDF, 23 mol % HFP, and 19 mol% TFE, while FT 2481 consists of 63 mol % VDF, 20 mol % HFP, and 17 mol % TFE.[61] The common sequence orders of FLS 2690 and FT 2481 are triads of VDF-HFP-VDF, TFE-HFP-VDF, and HFP-VDF-HFP, besides two adjacent VDF units. Both terpolymers contained traces of HFP-CH_2-CF_2 (VDF) and HFP-CF_2-CH_2 (VDF) sequences.

Isbester et al. also characterized two THV grades of different monomer compositions.[62] One was composed of 50.5% VDF, 22.8% TFE, and 26.7% HFP, while the other one consisted of 61.1% VDF, 20.9% TFE, and 18.0% HFP based on the molar percentage of the monomer feed rate. VDF-HFP-VDF, TFE-HFP-VDF, and HFP-VDF-HFP triads and VDF-VDF, TFE-VDF, TFE-HFP, TFE-TFE, and VDF-TFE dyads were evidenced.

Ok[63] repeated ^{19}F MAS NMR spectroscopy in i) solid-state, ii) in the molten state at elevated temperatures, and iii) solution in supercritical carbon dioxide (sc CO_2), at a critical temperature (T_c) of 31.1 ^{o}C and a critical pressure (P_c) of 73.8 bar.[64-66] For the third analysis, he developed a high-pressure NMR cell to conduct peculiar ^{19}F NMR measurements on THV in sc CO_2 solution.[63] Such a terpolymer has randomly distributed sequence orders.[63] There are adjacent TFE units in addition to the predominant occurrences of HFP-TFE-TFE sequences as well as -(CF_2-CH_2)-HFP-TFE-TFE, and some tetrads, such as TFE-VDF-TFE-TFE besides the VDF-HFP-VDF and TFE-VDF-HFP triads. Some of the weak correlations evidenced the presence of -CF_2-CH_2-$CF(CF_3)CF_2$- dyads. Furthermore, other sequence orders were identified, such as TFE-

HFP-TFE-TFE-VDF-HFP-VDF heptad and TFE-HFP-TFE-TFE-HFP-VDF hexad. Nearly 50 % of the TFE units are adjacent to HFP ones, while 20 % of TFE units are next to each other. The remaining TFE units are randomly distributed.

In another contribution by Ok et al.[67] using the equations in the literature[62] and integrating the peaks assigned to adequate groups such as CF_2 and CF_3 in the backbone of THV 221 G, the molar percentages of VDF, HFP, and TFE were 38.2, 10.4, and 51.4, respectively (Figure 9[68]) illustrating ^{19}F NMR spectra of PVDF and other FPs including THV). Some assignments, attributed to specific groups in VDF-HFP dyads and in TFE-TFE-TFE-HFP tetrad, were confirmed by gCOSY NMR spectroscopy.[69] In addition, 2+2 VDF ^{19}F NMR signals between -92 ppm and -95 ppm were noted in the ^{19}F-^{13}C gHSQC spectrum while 1+1 ^{13}C NMR resonances belonging to $–CF_2$ of VDF at ca. -119.00 ppm confirmed the expected VDF-TFE and HFP-VDF dyads.

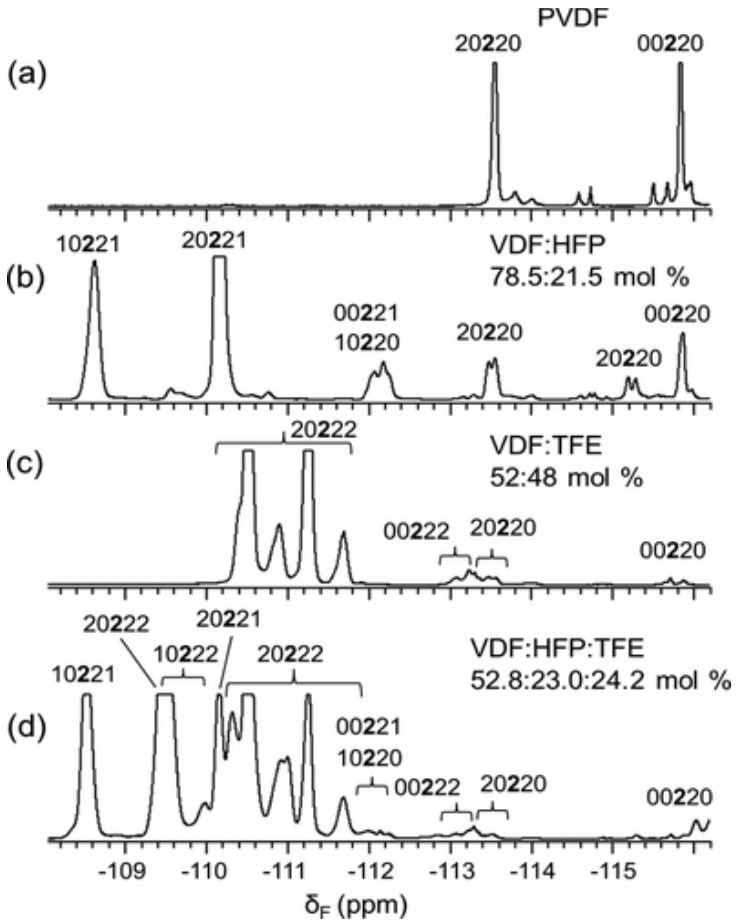

Figure 9. Expansion of -116 and -108 ppm of ^{19}F NMR spectrum for the comparison of the 022 3-carbon sequence regions from the 470 MHz 1D NMR spectra of (a) PVDF, (b) poly(VDF-*co*-HFP), (c) poly(VDF-*co*-HFP), and (d) THV terpolymer. The numerals 0, 1, 2, and 3 denote CH_2, CF, CF_2, and CF_3, respectively (reproduced with permission from ACS).[68]

Four of the five peaks of protonated carbons in VDF ranging between 25 and 45 ppm in the ^{13}C NMR spectrum were assigned to the methylene groups in -CF_2-$\underline{C}H_2$-CF_2-CF_2-$\underline{C}H_2$-$\underline{C}H_2$-CF_2-$\underline{C}H_2$-, while the fifth one was attributed to head-to-tail propagation as in the -CH_2-CF_2-$\underline{C}H_2$-CF_2- sequence order, with the signals between 30.80 and 44.50 ppm.

Twum et al.[68] concluded that for THV-A and THV-B terpolymers, approximately 92% and 91% of HFP monomers are adjacent to a VDF unit, respectively. No resonance was detected for HFP-HFP and either TFE or reverse VDF units that might succeed in the remaining HFP units.

The significant fraction of TFE-TFE units in terpolymer B might be attributed to more proneness of VDF monomer to react onto TFE units.[70] Microstructural analysis of poly(VDF-*co*-TFE)[71] and poly(VDF-*co*-HFP)[56, 72] copolymers clarified various sequence orders of the two THV terpolymers up to five and seven carbons with the following examples: -CF_2-(CH_2-CF_2)[$CF(CF_3)$-CF_2)]- and -CF-(CH_2-CF_2)-[$CF(CF_3)$-CF_2]-. THV-B has the sequence orders of -CF-(CH_2-CF_2)-(CF_2-CF)-; -(CF_2-CH_2)-(CF_2-CF_2)-CF_2-; -(CF_2-CH_2)-(CF_2-CF_2)-$CF(CF_3)$ with high concentrations, and the sequences of -CH_2-(CH_2-CF_2)-(CF_2-CF_2)- and -CH_2-(CH_2-CF_2)-[CF_2-$CF(CF_3)$]- with lower fractions. Various dyads, such as VDF-HFP and VDF-TFE, where VDF could be either -CH_2-CF_2 or -CF_2-CH_2- are also observed, as well as the following sequences: VDF-VDF-HFP-VDF; TFE-VDF-HFP-VDF; TFE-$(VDF)_3$; HFP-$(VDF)_3$; TFE-$(VDF)_2$-HFP; (VDF-TFE)$_2$ tetrads.

THV is a statistical terpolymer with a finite alternating portion. The microstructural analysis of THV is helpful in two crucial aspects: i) gaining insight into a better understanding of the synthetic reaction routes to free radical terpolymerization of VDF, HFP, and TFE units, and ii) correlating macro-properties such as enhancement in

hydrophobicity of the THV terpolymer to its microstructure.[73]

Table 2 lists the peak assignments of the ^{19}F-NMR spectrum of THV acquired in the solid-state MAS NMR.[63] Two CF_3 peaks in HFP units are explained by different local chemical environments. The peaks of CF_2 groups in HFP range between -103.0 and -119.0 ppm, while those of CF_2 of TFE are between -121.0 and -126.0 ppm.

Table 2. Peak assignments in 1D ^{19}F MAS-NMR spectrum of THV.[63, 68-69]

Groups	δ ^{19}F (ppm)
CF_3 (HFP): $CF(C\boldsymbol{F_3})CF_2$-$CF_2CF_2$-	-71.6
CF_3 (HFP): $CF(C\boldsymbol{F_3})CF_2$-$CH_2CF_2$-	-76.5
CF_2 (VDF)	-89.8
CF_2 (VDF-trans conformation)	-98.1
CF_2 (HFP): $CF(CF_3)C\boldsymbol{F_2}$-$CH_2CF_2$-	-103.9
CF_2 (HFP)	-109.3
CF_2 (HFP)	-112.0
CF_2 (HFP)	-114.9
CF_2 (HFP): $CF(CF_3)C\boldsymbol{F_2}$-$CF_2CH_2$-	-118.5
CF_2 (TFE)	-121.8
CF_2 (TFE)	-123.5
CF_2 (TFE)	-125.8
CF (HFP)	-182.2
CF (HFP)	-184.2

2.3 Average Molar Mass Determination (M_w)

Because PTFE is poorly solubilized, assessing molar mass is quite difficult by conventional methods such as size exclusion chromatography (SEC) and viscosimetry. However, the presence of side chains brought by comonomers (e.g., CF_3 in HFP and the alkyl group from vinyl ethers) reduces the crystallinity and hence increases the solubility of the resulting co- or terpolymers.

The composition of poly(TFE-*ter*-P-*ter*-GVE) terpolymers synthesized by Eguchi[22] varied from 40-50 mol.% of propylene (P), 50-60 mol.% TFE, and 0.01-10

mol.% of glycidyl vinyl ether (GVE). The preferred number average molar mass (M_n) values were claimed to range from 20,000 to 100,000 g/mol, while M_n values were between 30,000 and 80,000 g/mol when thin films with cross-linked possibility were generated.

Baradie and Shoichet[25] reported that M_w, M_n, and PDI of poly(TFE-*ter*-VAc-*ter*-VA) terpolymers were 296 kg/mol, 127 kg/mol, and 2.33, respectively. The molar mass shifted to a lower value due to the hydrolysis of poly(TFE-*co*-VAc) into poly(TFE-*ter*-VAc-*ter*-VA) terpolymer, inducing a peak of small intensity to a high molar mass tail in the SEC chromatogram with both M_w and PDI increases.

M_w and M_n values of a copolymer based on TFE and a trifluorovinyl acetate comonomer (FAc) were in the 3300-3170 and 4900-5200 g/mol ranges (in equivalent poly(methyl methacrylate), PMMA) and thus much underestimated, depending on the copolymer composition.[40] Only 10% of each copolymer showed relatively higher M_n ranging from 7200 to 9800 g/mol. The PDI of the terpolymers was ca. 1.5.

Maccone et al.[74] investigated the PDI of branched THV samples (based on VDF (71.5 mol.%), HFP (18.0 mol.%), and TFE (10.5 mol.%)) under the Tecnoflon® P757 trademark marketed by the Ausimont company (now Syensqo) prepared from a "branching and pseudo-living technology",[75-77] by combining SEC results with the intrinsic viscosity values of the polymer. These THV samples had trifunctional LCBs derived by the conversion to polymer mechanism.[74| PDI values of linear THV samples were broader than those of branched ones[74] while the linear ones had a lower M_w fraction. Fractionated samples had higher intrinsic viscosity than the corresponding full samples. For a branched THV, there was no correlation between the hydrodynamic volume and the average M_w because the hydrodynamic volume of the polymer chain relies on the LCB number. The Ram-Miltz approach[78] highlighted that the sample involving the diolefin had higher branches per macromolecule than the other ones. Fractionated samples had as low as 0.48 number average branching per macromolecule of tri-functional. The sample with the olefin had 1.70 of average LCB per macromolecule of both tri- and tetra-functional. The first three fractionated samples increased from 0.2 to about 1.5 branches per macromolecule by increasing the M_w of the polymer. THV with the olefin contained a higher branching repetition from 0.5 to 4 units per terpolymer

chain. The form of the PDI in the high M_w zone proves the existence in the polymer of a population of very high M_w originating from the LCB generated by the diolefin (sample D of Figure 10).

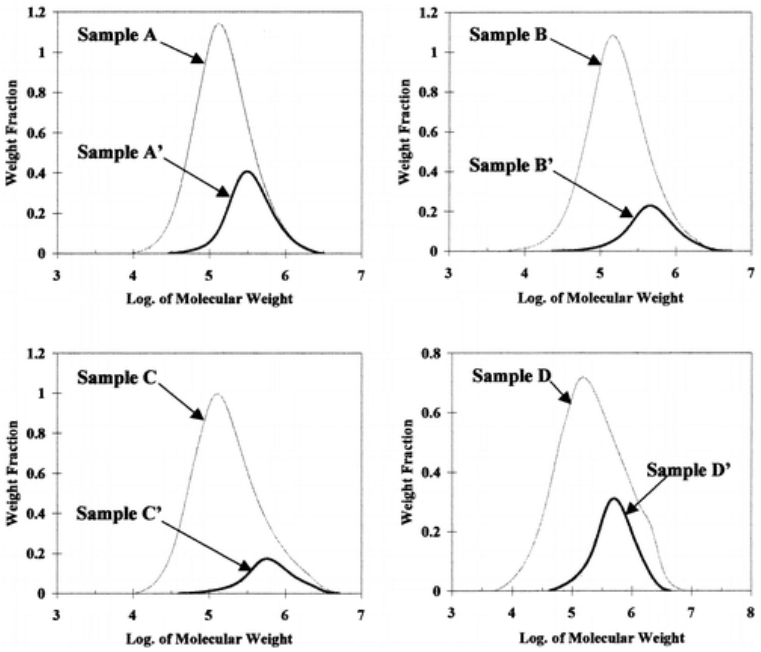

Figure 10. Size exclusion chromatograms of the polymers with the composition of 72/18/10 mol % for VDF, HFP, and TFE monomers, respectively. Thin lines: PDIs of samples A-D). Thick lines: PDIs of the high molar mass fractions produced by polymer fractionation (samples A'-D').[74] Polymers A-C were synthesized by the pseudo-living method, while sample D was prepared by a controlled mass of a fluorinated diolefin (branching & pseudo-living technology).[75-77] The high molar mass fraction of samples A-D is labeled A'-D' (reproduced with permission from Soc. Anonima Ed. di Chimica).).[75]

Stange et al.[79] continued the efforts of Auhl et al.[6] and utilized ten linear and six LCB terpolymers with 39 mol.% TFE, 11 mol.% HFP, and 50 mol.% VDF. The controlled incorporation of LCB yielded THV probes with a complex thermo-rheological behavior. The zero-shear rate viscosity (η_0) of a fraction of the LCB THV samples was more remarkable than that of a linear THV with the same M_w. Moreover, M_c, "the critical

molar mass" for the entanglement of random branches, is 2.5 times higher than the molar mass for entanglements, M_e, calculated as 4100 g/mol.[79]

3. Properties of TFE Terpolymers

3.1 Influence of Radiation on TFE Terpolymers

Radiation has also been utilized to synthesize modified TFE terpolymers. One example is reported by Kostov et al.[30] who terpolymerized TFE with propylene (P) and n-butyl vinyl ether (NBVE) initiated by γ-rays at room temperature and by varying the NBVE initial molar ratio. Various poly(TFE-*ter*-P-*ter*-NBVE) terpolymers were produced with 50 mol.% of TFE. The polymerization rate and M_w increased with the NBVE comonomer feed content. Transparent rubber-like terpolymers were obtained independently of the feed composition. The thermal and chemical resistances slightly decreased as the NBVE increased. T_g values of terpolymers were sharply reduced.

Dessouki et al. processed membranes by direct radiation-activated graft polymerization of acrylic and methacrylic acid (as hydrophilic monomers) solutions on THV thin films.[80] The water-absorbance percent increased as the grafting increased, and both the alkali untreated and treated films had higher water uptake, evidencing such a grafting. The swelling level relies mainly on the portion of the hydrophilic groups in the grafted THV films. The modification of free carboxylic acid functions of the grafted thin films into their K-salt introduced electrolytic groups conferring an ion nature. The conductivity of the KOH-refluxed grafted films was greater than that of the non-refluxed samples. The electrolytic groups originating from the alkaline treatment increased the transportability of the ionic species and enhanced the electrical conductivity.

Perm-selective membranes were obtained by grafting THV with N-vinylpyrrolidone (NVP) *via* gamma irradiation at a dose grade ranging from 1.04 to 1.24 Gy/s.[81] The monomer concentration increase enhanced the degree of grafting. At the first irradiation step, the grafting level increased with irradiation duration at a given NVP concentration. At greater dose rates, gel permeation hinders monomer diffusivity. The fraction in water absorbance increased continuously with the increase in grafting for all grafted THV thin films. The increase in the grafting level improved the electrical

conductivity but reached a level off above 10%-grafting. The permeability measurements with the membranes of grafted THV films conducted for lead (Pb) acetate solutions indicated increased permeates' concentration with the grafting level. Radiation-grafted THV membranes could be utilized for removing fractions of heavy metal ions such as Pb^{2+} from wastewater.

The THV terpolymers of THV-200, THV-400, and THV-500, upon irradiation with doses of 50 kGy at three temperatures ranging from 25 to 125 ^{o}C under reduced pressure (< 10^{-2} Pa),[82] carried approximately the same T_b, but E_b was reduced with decreasing VDF content as follows: THV-200 > THV-400 > THV-500. Upon irradiation at room temperature, both T_b and E_b decreased with chain scission. Irradiating the THV samples at high temperatures resulted in a bit of T_b enhancement. E_b indicated almost a steady degree in the experimental uncertainty range. Electron paramagnetic resonance (EPR) spectroscopy highlighted a decrease in the percentage of trapped radicals with elevation in irradiation temperature and by increasing VDF content: THV-500 > THV-400 > THV-200.

3.2 Microstructure-Property Relationship in TFE Terpolymers

Schmiegel[31] studied the characteristics of TFE terpolymers after 13 day-exposure of poly(TFE-*ter*-P-*ter*-VDF) and poly(TFE-*ter*-P-*ter*-TFP) terpolymers (where TFP is 3,3,3-trifluoropropene) to the strongly basic cyclic amidine base 1,8-diazabicyclo[5.4.0]undec-7-ene (DBU). Only ca. 15% of fluorine in poly(TFE-*ter*-P-*ter*-TFP) terpolymer was generated, compared to poly(TFE-*ter*-P-*ter*-VDF). Poly(TFE-*ter*-P-*ter*-TFP) with 76, 20, and 4 wt% of TFE, P, and TFP, respectively, was more than 6 times more resistant to DBU as poly(TFE-*ter*-P-*ter*-VDF) with 54, 14, and 32-wt% of TFE, P, and VDF, respectively. The high VDF content necessary for a satisfactory bisphenol crosslinking of poly(TFE-*ter*-P-*ter*-VDF) makes them less base-resistant than poly(TFE-*ter*-P-*ter*-TFP) because the TFP fraction is less prone to undergo dehydrofluorination.

In a report on the elastic modulus of a TFE-based terpolymer, Arai et al.[32] focused on the effect of side branches regarding the storage modulus (E') of ethylene (E)-TFE terpolymer based on dynamic mechanical tests. Ethylene and TFE were

terpolymerized with either HFP or 3,3,4,4,5,5,6,6,6-nonafluorohexene (NFH) *via* a radical initiation. The unit cell size of the resulting terpolymer did not vary significantly when the -C_4F_9 branches remained in the ETFE chains.[83] The -CF_3 branches were included within the crystal lattice, while the -C_4F_9 stayed in the amorphous domains or lamella outer topmost layer. Poly(E-*ter*-TFE-*ter*-HFP) terpolymers demonstrated a different behavior than that of poly(E-*ter*-TFE-*ter*-NFH) terpolymer. For the latter one, E' relied on the fraction of branches and crystallinity rate. In contrast, for poly(E-*ter*-TFE-*ter*-HFP) terpolymer, the modulus did not change remarkably even when the crystallinity varied significantly from 30% to 50%.[32] E' values of poly(E-*co*-TFE) and poly(E-*ter*-TFE-*ter*-NFH) were similar. The -CF_3 groups were inserted in the crystal lattice, resulting in its expansion, hence remarkably lowering the Young's modulus of the crystalline phase (Figures 11 and 12).

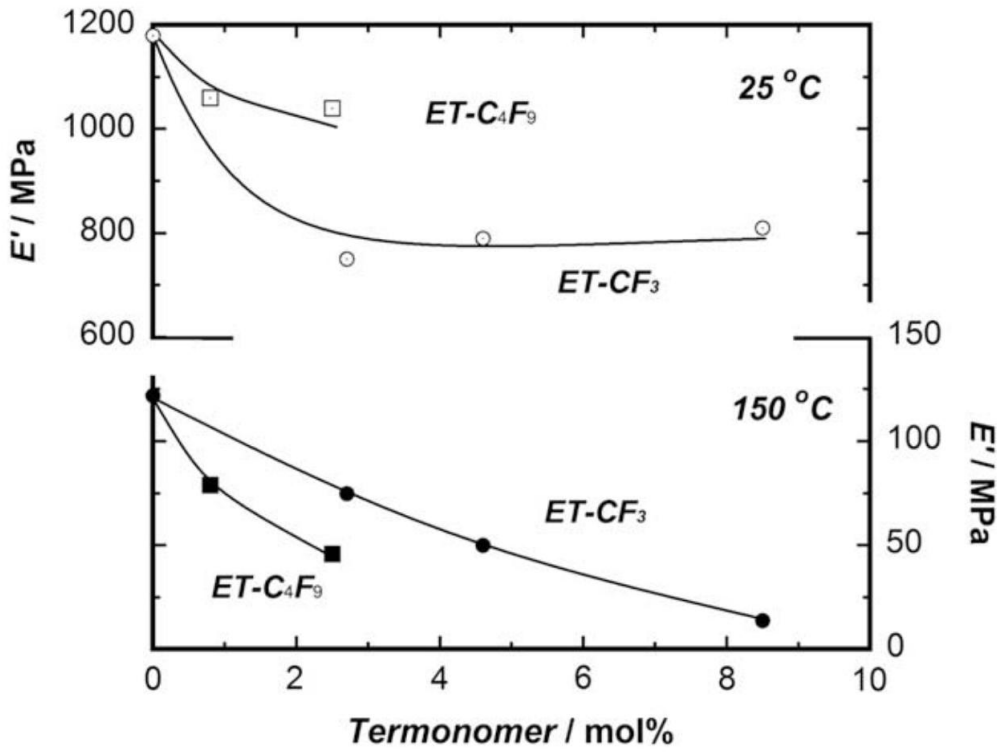

Figure 11. Termonomer content dependence of the storage modulus (E') at 25 and 150 °C measured for both terpolymers. ET-CF_3 and ET-C_4F_9 stand for poly(E-*ter*-TFE-*ter*-HFP) and poly(E-*ter*-TFE-*ter*-NFH), respectively (where NFH is 3,3,4,4,5,5,6,6,6-nonafluorohexene) (reproduced with permission from Elsevier).[32]

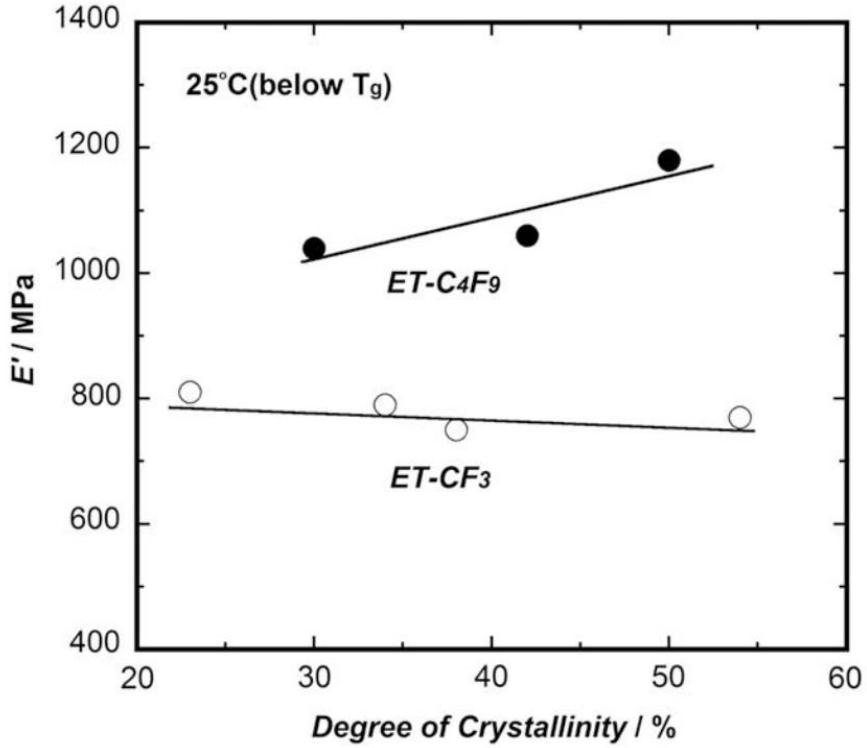

Figure 12. Dependence of E' on the degree of crystallinity at 25 ^{o}C for both terpolymers (a). Dependence of E' on the degree of crystallinity at 150 ^{o}C for the two terpolymers (b). ET-CF_3 and ET-C_4F_9 stand for poly(E-*ter*-TFE-*ter*-HFP) and poly(E-*ter*-TFE-*ter*-NFH), respectively (reproduced with permission from Elsevvier).[32]

In another effort, Funaki et al.[33] investigated the effect of a third monomer (HFP) or nonafluoro-1-hexene (CH_2=$CH(CF_2)_3CF_3$) on the phase-transition behavior of the uniaxially aligned ETFE-alternating copolymer. A solution-polymerization approach was used to synthesize the terpolymers, which were characterized by temperature-dependent measurements of X-ray fiber diagrams, small-angle X-ray scattering patterns, and polarized IR. The transition between low- and high-temperature phases happens discretely. A *trans-gauche* conformational disordering was evidenced in the high-temperature zone. The increase of the third monomer fraction resulted in a decrease in the phase-transition temperature (Figure 13).

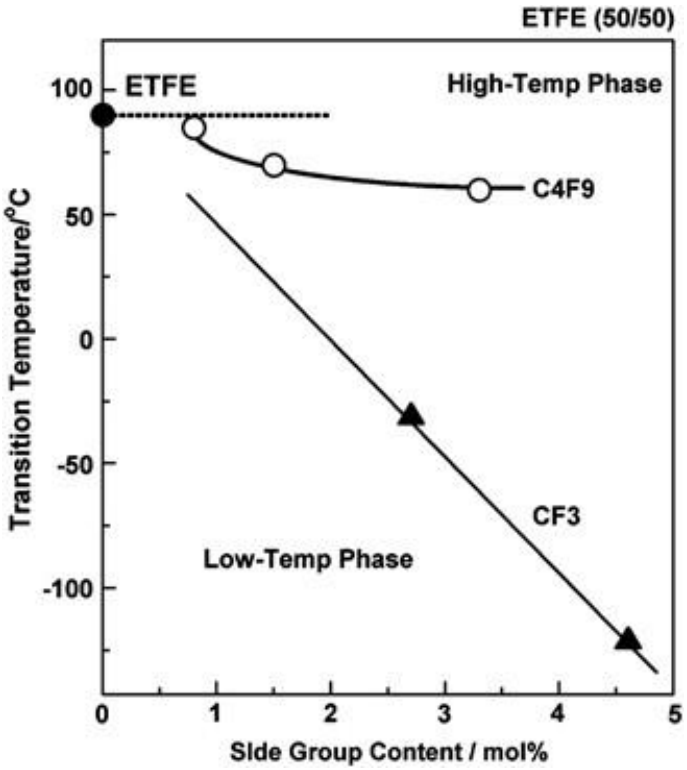

Figure 13. Transition temperatures of poly(E-*alt*-TFE) copolymer *versus* the molar content of the third monomer unit. The existence of a side group (C_4F_9) from 3,3,4,4,5,5,6,6,6-nonafluorohexene (NFH) does not influence the transition temperature remarkably, while the -CF_3 group in HFP lowers the transition point significantly (reproduced with permission from Nature Publishing).[33]

The rate for the decrease was more dominant in terpolymer-bearing short-CF_3 groups. Indeed, the side groups from the third monomers result in the enlargement of the unit cell dimension, inducing a shift in the order-disorder phase-transition temperature. However, the authors noted a mechanism change brought from -CF_3 to -C_4F_9 groups, where -CF_3 is included in the crystal lattice while -C_4F_9 groups are not. The insertion of -CF_3 groups in the crystal lattice caused an enlargement and a more remarkable shift in the transition temperature, even for low CF_3 fractions.[33]

3.3 Thermal Decomposition

Hiltz[48] characterized THV and poly(VDF-*co*-HFP) copolymer by pyrolysis(py)

GC/MS, FTIR, DSC and TGA. The Py-GC/MS method identified the polymers positively based on the variations in the pyrolytic degradation byproducts. Although FPs are thermally stable materials, they might start decomposition above their processing temperatures by, for example, pyrolysis, combustion, and incineration.[53] Among these methods, pyrolysis favors the decomposition of FPs involving either a glow or flames, sometimes releasing back some monomers. Incineration destroys a material *via* quite high temperatures and even fire. The decomposition of FPs usually yields fluoroalkanes, hydrogen fluoride, oxidation products, and FP particles.[84]

Among these copolymers, Hiltz[48] deeply studied FR17/75 fluoroelastomers based on TFE, HFP, and VDF, and LR6316/75 and FR25/80 containing TFE, VDF, and PMVE. The first elastomer could be utilized within a temperature varying from -12 and 210 ^{o}C, while the temperature ranges for the use of LR6316/15 and FR25/80 are between -29 and 205 ^{o}C, and from -41 to 200 ^{o}C, respectively. Among the fluoroelastomers of interest, FR17/75 exhibited the highest T_g of -13 ^{o}C whereas FR25/80 had the lowest one (-31 ^{o}C), attributed to variations in composition, microstructure, sequence orders, and additives.[47] The TGA results under N_2 displayed a weight loss of ca. 60% for LR6316/15 and FR25/80 elastomers at 505 and 497 ^{o}C, respectively, while FR17/75 elastomer had approximately 70% weight loss at the primary step at 501 ^{o}C. FR17/75 had a greater mass of residue than both LR6316/75 and FR25/80 fluoroelastomers, explained by the presence of fillers in the FR17/75.[48]

The fingerprints of the pyrogram of each fluoroelastomer were different. Figure 14 summarizes the possible ways to generate some of the ions in the mass spectra of FR17/75.

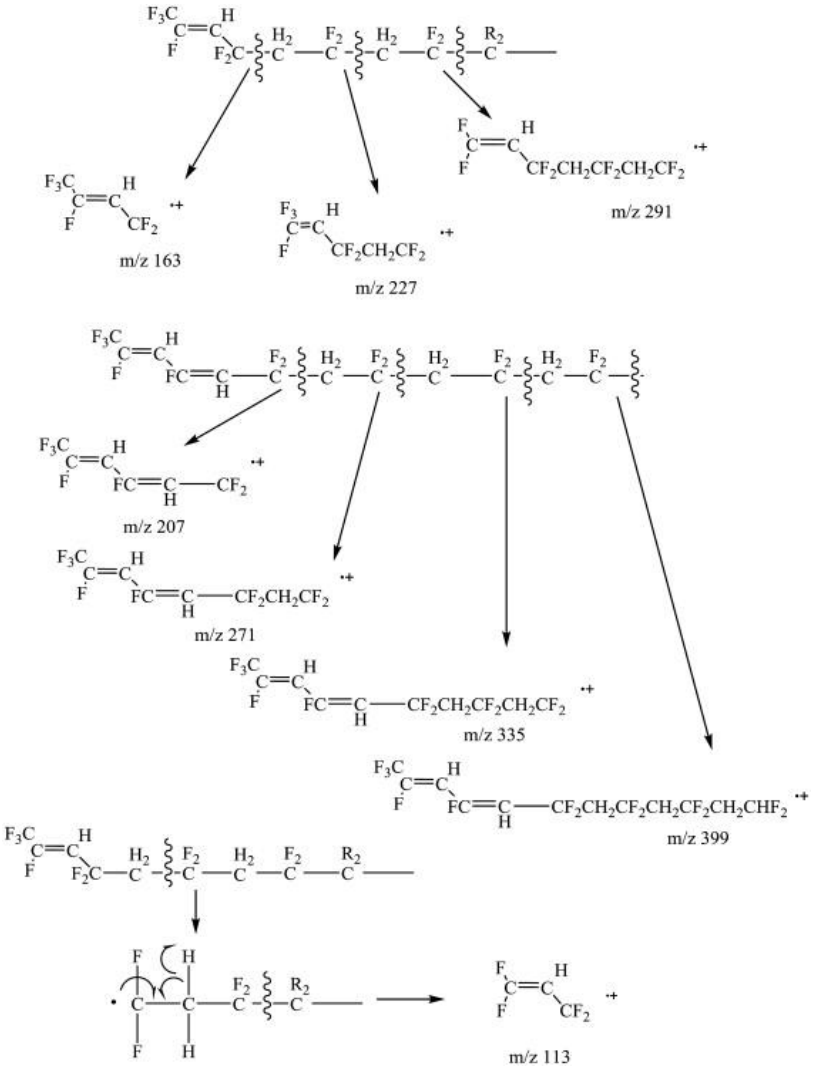

Figure 14. Possible paths of degradation of FR17/75 elastomer for the generation of some ions detected by mass spectrometry (reproduced with permission from Elsevier).[48]

The FR17/75 degradation products contained unique ions differing in mass by 20, 50, 64, and 100 units, arising from the loss of HF, CF_2, VDF, and TFE, respectively.

Poly(VDF-*ter*-TFE-*ter*-HFP) terpolymers are deformable materials without losing toughness. The distortion and morphology of THV having 52 mol.% VDF, 36 mol.% TFE and 12 mol.% HFP was reported by Freimuth et al.[85] who noted two relaxations: the first one at low temperatures, observed in the same temperature range of γ-relaxation of PVDF and PTFE due to local chain movements in the amorphous domains while the second one observed at elevated temperatures was explained by a ten-fold alteration in G'

occurring at a temperature close to the T_g. The stress-strain curve of THV at various temperatures is typical of a ductile polymer deforming by shear yielding. An intensive whitening is observed in the stress of THV, being stretched at T = 20 °C, showing cavitation plasticity at temperatures near T_g. The crystallinity rate (χ_c = 10%) of THV is lower than that of poly(VDF-*co*-TFE) copolymers ($\chi_c \approx$ 70-80%) but closer to that of poly(VDF-*co*-HFP) copolymers, where χ_c is as low as 5% (or 29%) for a copolymer containing 15.9 (or 2.9) mol.% HFP.[85] As in poly(VDF-*co*-HFP) copolymers, the incorporation of HFP units into the poly(VDF-co-TFE) backbone strongly reduces the crystallinity without altering the crystalline feature, as expected.[85] THV distortion at low drawing temperatures resulted in a four-point SAXS arrangement, transitioning to a two-point ordered structure as temperature increased. The slight long-period increase was attributed to THV crystalline lamella limited melting, occurring within its broad melting range around 120 °C.[86]

3.4 THV/Polymer Blends

Because of some possible difficulties in solubilizing FPs, THV blends with other polymers are scarce, and several articles report interesting blends composed of THV and other polymers.

First, Kaushiva et al.[87] investigated the structure-property relationships of PTFE/ THV blends (with THV based on a 14.9:65.2:19.9 molar ratio of TFE:VDF:HFP). The relative content of PTFE to THV was 0, 20, 40, 60, and 70 wt%. As a matter of fact, THV and PTFE were blended in emulsified, micro-particule forms and with the formulation of a curative agent, surfactants, and ionic surfactant ammonium caseinate in 10% dispersion, with a steady ratio of other compounds to THV. Above 100 °C, the hexamethylene diamine induced cross-links in fluoroelastomers via covalent bonds incorporating VDF in their composition.[88-89] The modulus data showed that the gap between the green leaf (non-treated) and the treated materials was only measurable at a more significant PTFE fraction. Still, post-treatment, the thermal curing promoting cross-linking above 100 °C, resulted in sufficient cross-linking to enhance the modulus

considerably. For instance, the post-treatment improved the modulus with all the fractions of PTFE by approximately 120% over the modulus of the non-treated samples.

The stress-strain behavior of the "green leaf" materials revealed two systematic tendencies: as the PTFE fraction was enlarged, the modulus increased, and the strain at break decreased. In the case of treated and post-treated materials, as in the green-leaf films, the moduli of the materials methodically increased with the increase of the PTFE fraction. Contrarily to the green-leaf materials, the strain at break is considerably dissimilar. For the treated materials, the strain units for samples with 20-60 wt% PTFE were two-fold higher than those with 0 wt% PTFE. Suitable PTFE fraction and cross-linking enabled the enhancement of the rubbery moduli of the films and the reduction of the size of the tan δ peak at 1.4, matching the T_g of THV. The magnitude of the tan δ peak reduced methodically as the THV percentage was decreased or with increasing cross-linking of THV. For the distortion rate used, a peak in the toughness of the materials was noted closer to 18 ^oC, considered to arise from a peak in the transfer of shear stress to the PTFE particles. There was a scattered morphology for the PTFE particulate, with THV establishing an uninterrupted matrix, where the PTFE particles of 0.2 μm were slightly aggregated. Even at 80 wt% PTFE, THV formed a continuous matrix.[87]

Möller et al.[90] focused on the effect of LCBs on non-linear rheological characteristics of THV, the shear, and the transient elongational viscosities. The soluble THV consists of 39 mol.% TFE, 11 mol.% HFP, and 50 mol.% VDF and the insoluble THV comprises 56 mol.% TFE, 12 mol.% HFP, and 32 mol.% VDF. The three soluble LCB THV demonstrated a more effective shear thinning than the linear soluble THV samples. The THV probe with the greatest branching shows the polymerization parameters with the highest strain-hardening coefficients: 1.6 and 1.7 with the same elongation rates of 0.03 s^{-1} at 180 and 265 ^oC, respectively. In insoluble THV samples, the blend of linear THV (85%) and LCB THV (15%) displayed a more effective shear thinning than the insoluble linear THV-L1, along with an important strain-hardening attitude (Figure 15). The polydisperse insoluble linear trimodal THV-L2 exhibited both strain hardening and pronounced shear thinning, proving the existence of LCB. Shear-

thinning in fluorinated thermoplastics could be obtained by either a high PDI or the integration of LCBs. For strain hardening, LCBs are needed.

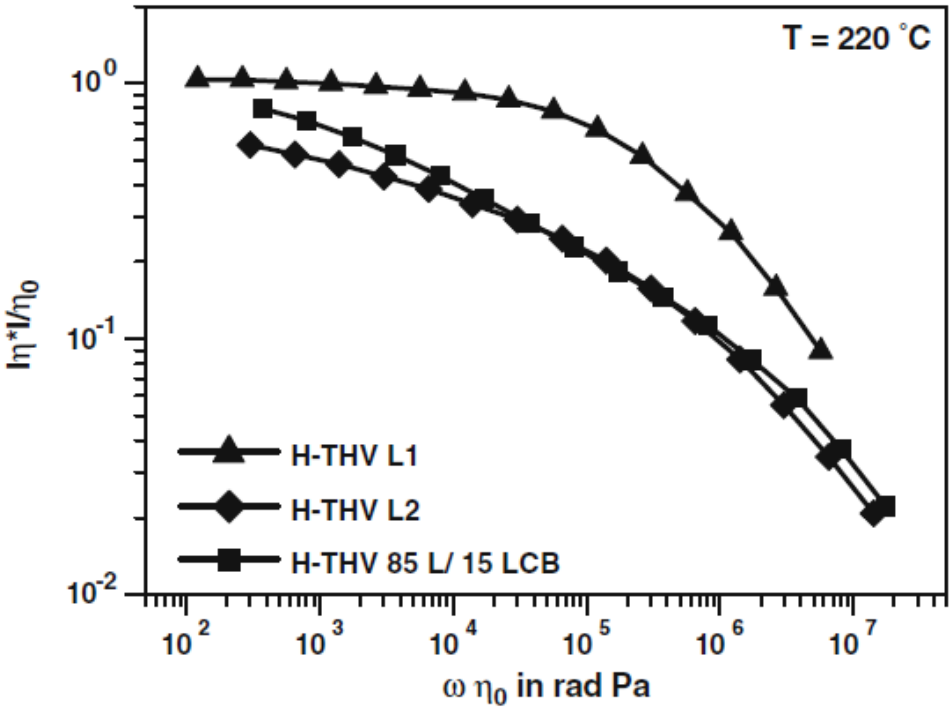

Figure 15. The normalized absolute value of the complex shear viscosity of the linear H-THV 85 / 15 LCB blend compared to the two linear H-THV samples (reproduced with permission from Springer).[90]

Kaspar and Hintzer[91] also studied the uniaxial extensional rheology property of 10 different LCB THV samples with the mole percentages of 39%, 11%, and 50% for TFE/HFP/VDF at 265 ^oC utilizing the extensional viscosity fixture. Within the extension rates between 0.03 $s^{-1} \leq \dot{\varepsilon} << 30\ s^{-1}$, the LCB THV probes exhibited weak to remarkable strain-hardening tendencies varying as a branching degree from 0.2 to 1.7. The experimental results demonstrated that the elongation stress response time (τ) relied on the size dimension of branching (λ), with a relationship of $\tau \sim \lambda^{3.3}$ as derived from molecular characterization (Figure 16).

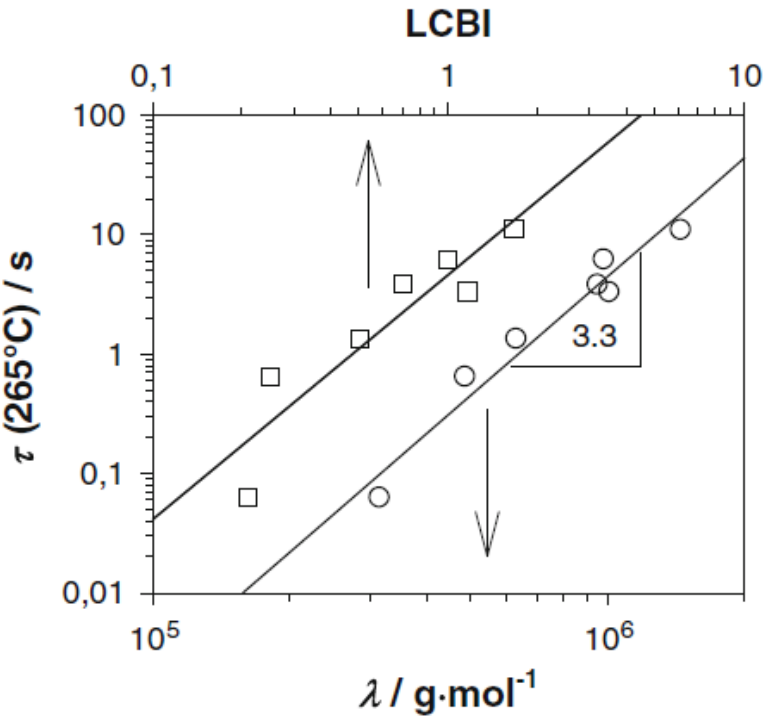

Figure 16. Elongational stress response times τ recorded at 265 °C and plotted by varying molar mass of tri-functional monomer unit λ (see Figure 17) of the long-chain branched THV samples ($TFE_{39}/HFP_{11}/VDF_{50}$) (reproduced with permission from Springer) .[91]

Note that τ also depends on the temperature, while λ enables to determine the branching units M_{arm}/M_e (Figure 17 presents a schematic of LCB macromolecule).

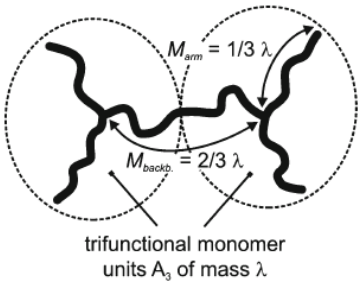

Figure 17. Schematic representation of an LCB macromolecule made up of two tri-functional monomer units (A3-type) of the average molar mass λ (reproduced with permission from Springer) .[91]

Siengshien and Abraham[92] studied the morphology and rheology of blends from high-density polyethylene (HDPE) and two THV samples, THV 220 and THV 500,

because fluorinated thermoplastic mixtures are cost-effective substitutes for engineering polymers in producing automobile fuel tanks.[93] Indeed, the rheological properties of the HDPE/THV500 blend differ from those of the HDPE/THV 220 blend. The dynamic linear viscoelastic characteristic- G' and viscosity of the HDPE/THV 500 blend were higher than those of the HDPE/THV 200 mixture, explained by the gap in the M_w and particle size distribution of THV probes. The parsimonious and modified Cox-Merz descriptions explain the modulus and viscosity outcomes (Figures 18 and 19). The influence of the M_w of THV samples on the crystallization kinetics of the blend is insignificant. There was a better dispersion of THV 200 particles into the HDPE matrix than in THV 500.

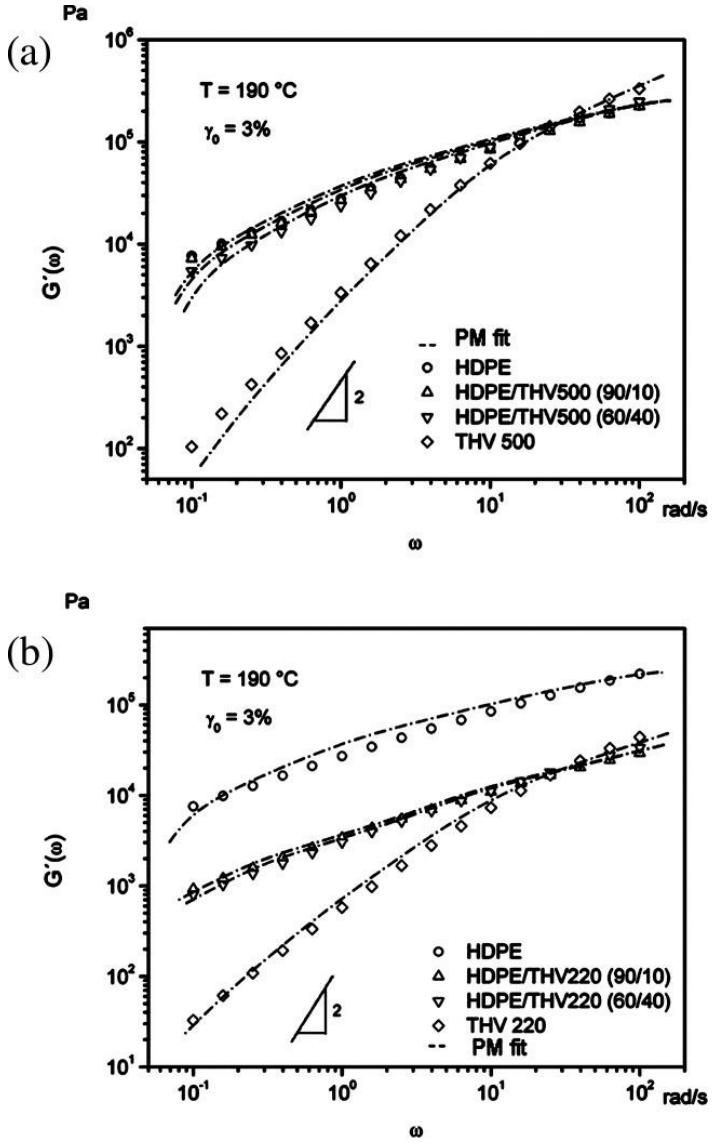

Figure 18. G' versus frequencies at T = 190 ^{o}C and their fitting by the parsimonious equation for HDPE/THV500 blends (a) and HDPE/THV220 blends (b), with ratios of HDPE/THV (90/10) and (60/40) (reproduced with permission from Wiley).[92]

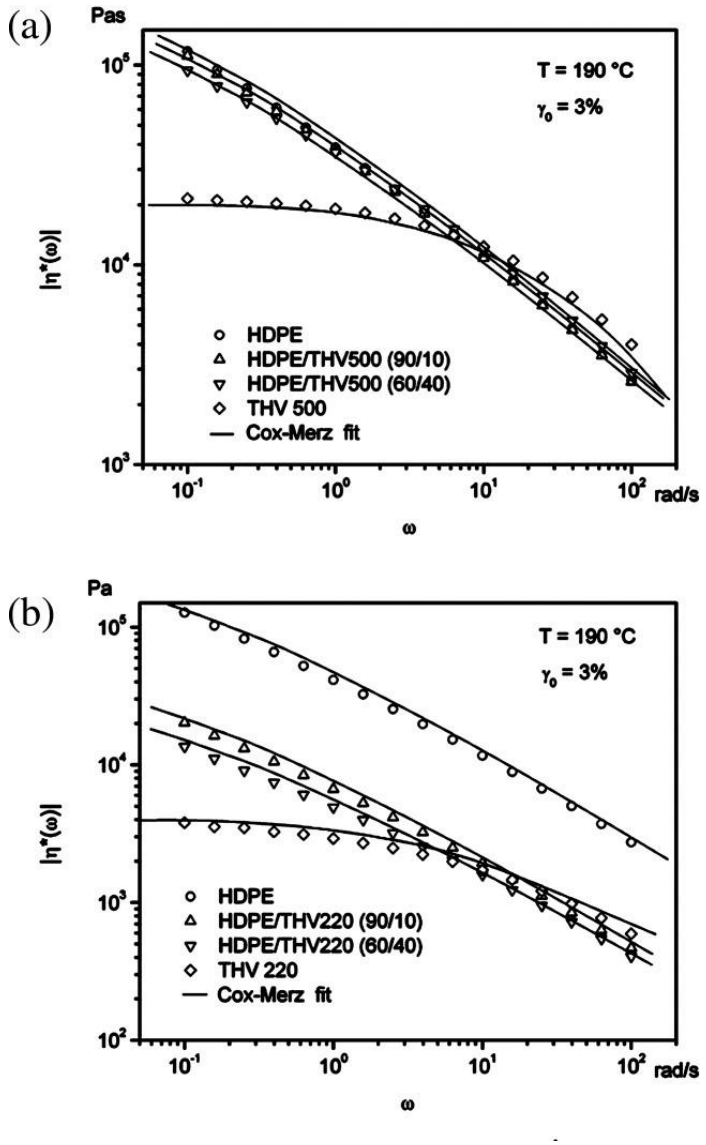

Figure 19. Viscosity versus frequencies at T = 190 ^{o}C and their fitting by the modified Cox-Merz rule for HDPE/THV500 blends (a) and HDPE/THV220 blends (b), with ratios of HDPE/THV (90/10) and (60/40) (reproduced with permission from Wiley).[92]

Recently, Khanra et al.[94] studied the effectiveness of methyl vinyl silicone-*g*-maleic anhydride (MVQ-*g*-MAH) for the compatibilization of Viton® GBL 200S, a THV-based fluoroelastomer with the methyl vinyl silicone rubber (MVQ) to generate a

"super specialty elastomer blend" with enhanced mechanical and thermal aging. MVQ-*g*-MAH is a compatibilizing agent, adjusting the interface between the polymer components and lowering the interfacial tension.[95] MAH was successfully grafted onto the silicone rubber, and then the MAH moiety of the MVQ-*g*-MAH was dispersed into the fluoroelastomer phase while the MVQ counterpart strengthened the interfacial adhesion. Out of different loadings of MVQ-*g*-MAH ranging from 0 to 10 parts per hundred (phr), 2 phr were the optimum one for which the fluoroelastomer/silicon rubber [50/50 (w/w)] blend obtained the most remarkable characteristics. There were enhancements in the blends' mechanical, thermal, and aging tendencies, proving the efficacy of the (MVQ-*g*-MAH) compatibilizer.

3.5 THV/Filler Composites

Nanocomposites based on FPs and fillers[3, 5-6, 14, 44] have also led to several examples. Researchers extended their efforts to the formation of fluoroelastomers-based nanocomposite materials. The primary goal of these contributions was to test the thermal and mechanical properties of such resulting materials. First, THV fluoroelastomer, namely Viton® A-500, commercially available from the Chemours Company (and formerly produced by Dupont Performance Elastomers), was also studied in nanocomposites. Kader and Nah[35] reported the effects of gum, montmorillonite (Na-MMT), and organo-modified MMT (Cloisite 15A) on the vulcanization kinetics of Viton® nanocomposites. For the vulcanization of elastomer, clay was first incorporated, and then hexamethylenediamine carbamate (DIAK 1) was added at the final stage to favor cross-linking. A change in *d*-spacing of Na-MMT toward greater values from 31.5 to 36.4 Å, as revealed by the X-ray diffraction form of the clay mineral-packed fluoroelastomer, indicated the establishment of the intercalated silicate layer. TEM images indicated the existence of an intercalated/exfoliated state of Na-MMT with stacks of platelets containing a limited number of layers included in the Viton-A 500 matrix. When the amount of the curative was increased, the remarkable enhancement in the treatment rate displayed the availability of curative for the treatment reaction. The determined activation energy of melt flow obtained from both rheometer (52.36, 70.83,

and 37.95 kJ/mol for Viton A500, Viton A500/Na-MMT, and Viton A500/O-MMT, respectively) and DSC (56.83, 72.18, and 39.18 kJ/mol for Viton A500, Viton A500/Na-MMT, and Viton A500/O-MMT, respectively) measurements, being closer to each other, demonstrated the efficiency of the organo-clay in decreasing the energy required for the vulcanization process. The characteristics of the clay is a major influential factor in the vulcanization of the fluoroelastomer.

Kader et al.[96] utilized melt mixing to prepare Viton-A 500/layered clay (Na-MMT and organically modified clay (OMMT)) nanocomposites, studied the dispersion of the clay minerals, and characterized morphological, rheological, and thermal properties of the composites. The percentages of Na-MMT in the composites were 2.5, 5, 10, and 15 wt.%, while those of OMMT in the composites were 2.5, 5, 10, 15, and 20 wt.%. The existence of intercalated/exfoliated clay strata with good spreading at smaller fractions of embedded filler was revealed by TEM measurements (Figure 20).[96]

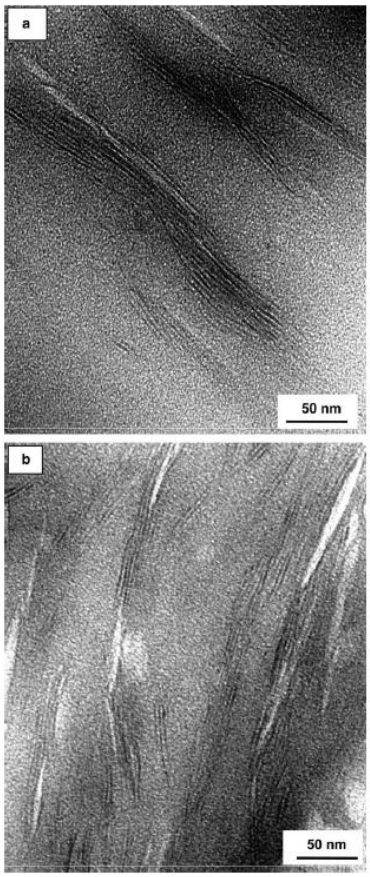

Figure 20. High magnification TEM image of (a) THV/Na-montmorillonite intercalated nanocomposite (mass fraction of Na-montmorillonite is 5 wt%) and (b) THV/organically modified-montmorillonite intercalated/exfoliated nanocomposite (mass fraction of organically modified-montmorillonite is 20 wt%) (reproduced with permission from Elsevier).[96]

Although the pristine fluoroelastomer and fluoroelastomer/clay nanocomposites indicated a shear-thinning behavior and temperature reliance on shear stress, the shear viscosity of the polymer/OMMT nanocomposites was smaller than that of the pure polymer at all temperatures and shear rates. The composites indicated easier processing. Adding layered clay enhanced the T_g of Viton®-A 500, and the thermal steadiness of the fluoroelastomer became better with the unmodified clay addition. On the contrary, in the case of OMMT, the initial degradation temperature was reduced due to the decomposition of the organic constituent of the modified clay mineral.[96]

Maiti and Bhowmick[97] comprehensively developed a series of studies devoted to interesting preparations of Viton®/clay composites. First, VitonB-50/Na-MMT clay composites were achieved from solution in MEK first, then dispersing the clay by varying the concentrations from 5 to 25 wt%. XRD patterns of the composite materials showed no peak in 2^o-9^o for solution concentration up to 20 wt%. The absence of any peak up to 20 wt% highlights exfoliations of the clays up to 20%. Above 20 wt% concentration, the terpolymer chains intercalate in the galleries of the clay particles, as highlighted by the AFM results. At small concentrations such as 5 wt%, poor mechanical properties of composites were observed despite exfoliation of the clay particles. The explanation is the de-coiling of the polymer chains where the chains are separately solvated, yielding an enhancement in hydrodynamic volume. A higher concentration of the polymer solution results in the inhibition of the exfoliation. Tensile characteristics are the best at 20 wt%, where the G' modulus of the film is at its greatest value. The improved properties of the films at 20 wt% are attributed to the interaction between the polymer and filler.

The same group[98] investigated the dynamic viscoelastic properties of Viton® B-50 nanocomposites with clay minerals (Na-MMT and OMMT, Cloisite 20A) from 20

wt% solutions in ethyl methyl ketone. Variations in T_g and G' were observed with the dispersion of modified and unmodified nanofillers, where tan δ peak heights decreased, and G' increased, especially with unmodified clay minerals. Increasing nanofiller loading slightly enhanced G' but did not significantly affect T_g and tan δ. The presence of nanoclays shifted crossover points in G' and complex viscosity (η*) plots to higher frequencies. α-crystallization in Viton® B-50 showed increased G' in nanocomposites after 0.2% strain, with strain sweep measurements revealing an overturn in G' around 0.2% strain regardless of nanofiller presence. Uniaxial strain prior to DMA measurements influenced storage modulus (E') and α-phase crystal pattern in VDF monomers, confirmed by clay mineral layer alignment observed via wide-angle XRD and TEM studies. Additionally, the same authors[99] examined the influence of Viton® B-50 and clay particle interaction on solvent (MEK and THF) diffusion and sorption in elastomer/clay nanocomposites, determining nanoclay aspect ratio. Swelling measurements at 30-60°C indicated slightly non-Fickian diffusion for Viton® B-50/clay nanocomposites, with diffusion coefficient reductions for MEK with both unmodified and modified clay loadings. Higher clay mineral content led to decreased diffusion coefficients, attributed to maze-like structure formation. Nanocomposite samples exhibited re-swellability, with Fickian diffusion upon re-swelling due to stronger polymer-clay interactions retarding solvent diffusion.

Mali et al.[100] and Shimpi et al.[101] also reported Viton® E-60C/OMMT nanocomposites, the mechanical of which were deeply studied: the tensile strength was enhanced nearly 3.2 times, while elongation at break increased from 500 to 600% compared to that of pristine Viton® when the loading of surface-modified OMMT was 9 wt%. In addition, the addition of Viton® chains with wetting capability between the OMMT plates favored the remarkable improvement in thermal stability of OMMT-filled nanocomposites. At 12 wt% OMMT filling, the properties of Viton®/OMMT nanocomposites worsened due to the OMMT agglomeration as evidenced by SEM and AFM results.

The same team[101] utilized the identical probes as previously.[100] and studied photo-oxidative degradation of the nanocomposites under accelerated UV (λ = 290.0 nm) irradiation as a function of time (Figure 21). They observed a progressive decrease of the

mechanical, thermal, and physical properties of the composites as the UV exposure time was prolonged, assigned to a reduction of the degree of cross-linking with enhancement in rubber chain mobility. FTIR results evidenced the increase in >CO and –OH groups in the nanocomposites by the UV exposure time from 0 to 300 h. Viton®/OMMT nanocomposites were influenced more than pristine Viton® by the UV irradiation. This result was more pronounced when the surface-modified OMMT loading was 12 wt% for a UV exposure time of 300 h.

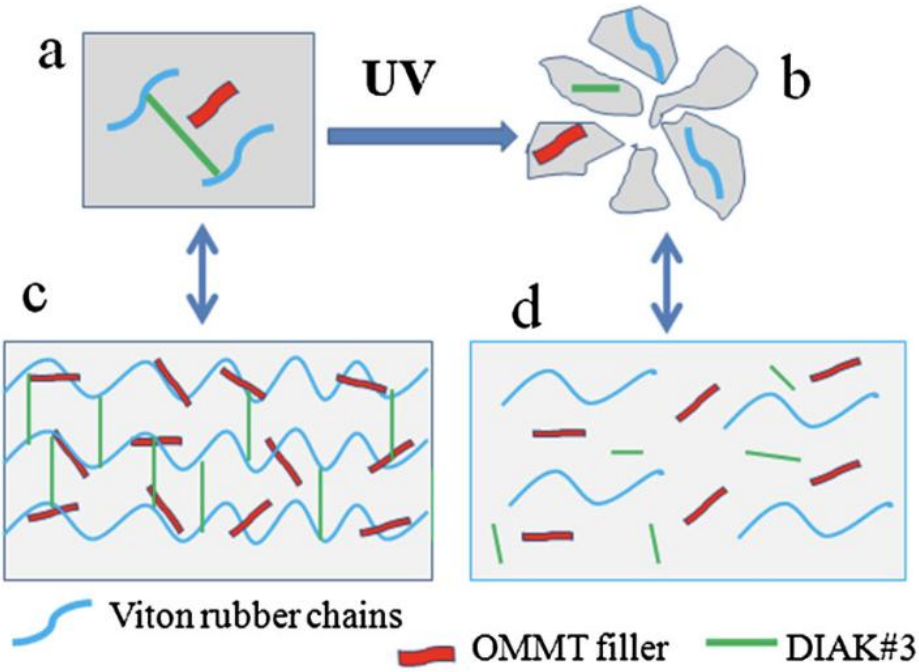

Figure 21. Schematic of the concept of UV light degradable nanocomposites based on Viton and OMMT before (a, c) and after (b, d) UV exposure (reproduced with permission from Wiley).[101]

Zen and Lugao[102] investigated the influence of the OMMT derivative, Cloisite 15A, integration in the dimensional steadiness of the elastomeric matrix. Because Viton® F has been used in generating O-ring, preserving the material size steadiness is relevant. The goal of using OMMT was to overcome possible swelling issues of Viton® F. The elongation at break and swelling rate were reduced, related to the enhancement in cross-linking and the establishment of networking in the nanocomposites.

In a series of publications, Heidarian and Hassan[103-105] extensively focused on using carbon nanotube (CNT) and Viton® GF-600S to obtain composite materials. T_g of Viton®/CNT was significantly increased compared to that of Viton®/Carbon black (CB) or unfilled Viton®. A higher G' was also observed for Viton®/CNT nanocomposites. The most contrary remarkable result was a smaller tan δ in the glassy form and larger in the rubbery state. Both unfilled and filled Viton® demonstrated crystallinity, as α-form crystalline of pristine Viton® and Viton®/CB nanocomposites. γ-crystallinity was induced by shear and elevated temperature in Viton®/CNT nanocomposites.

Continuing their efforts, the same group[104] first modified surface carbon nanotube (MCNT) with acid (with -COOH Content: 0.49 wt.%), then prepared Viton® GF-600S/MCNT nanocomposites. DMA measurements indicated that T_g value of Viton® GF-600S (surprisingly high, 13 ^oC) was slightly enhanced in CNT/ Viton® GF-600S composites (17 ^oC) while similar in MCNT/ Viton® GF-600S composites (12 ^oC). Moreover, from DSC results (scanning rate of 100 ^oC/min), T_g of Viton® GF-600S (8.5 ^oC) was *quasi*identical to those of CNT/ Viton® GF-600S composites (8.6 ^oC) and in MCNT/ Viton® GF-600S composites (5.5 ^oC). A scanning rate of 10 ^oC/min yielded the same trend in the T_g of Viton® GF-600S (-6.9 ^oC) showed little change compared to those of CNT/ Viton® GF-600S composites (-2.6 ^oC) and in MCNT/ Viton® GF-600S composites (-3.6 ^oC). For the temperature range between -100 and +300 ^oC, G' of Viton®/MCNT was also lower than that of Viton®/CNT. G' in the rubbery phase was higher for Viton®/MCNT than for unfilled Viton® (Figure 22). Furthermore, G' of Viton®/MCNT composite was slightly higher in the glassy phase than that of Viton®/CNT. Loss modulus (G") values, both glassy and rubbery states of Viton®/MCNT were lower than those of Viton®/CNT. Compared to pristine Viton®, the loss modulus of Viton®/MCNT in the rubbery state was higher, and in glassy states for both composites, the loss modulus was the same. The crystallinity of unfilled Viton® and filled Viton® were mainly in γ-phase, and this crystalline γ-form was in the following increasing order: Viton®/MCNT< Viton®/CNT<unfilled Viton®.

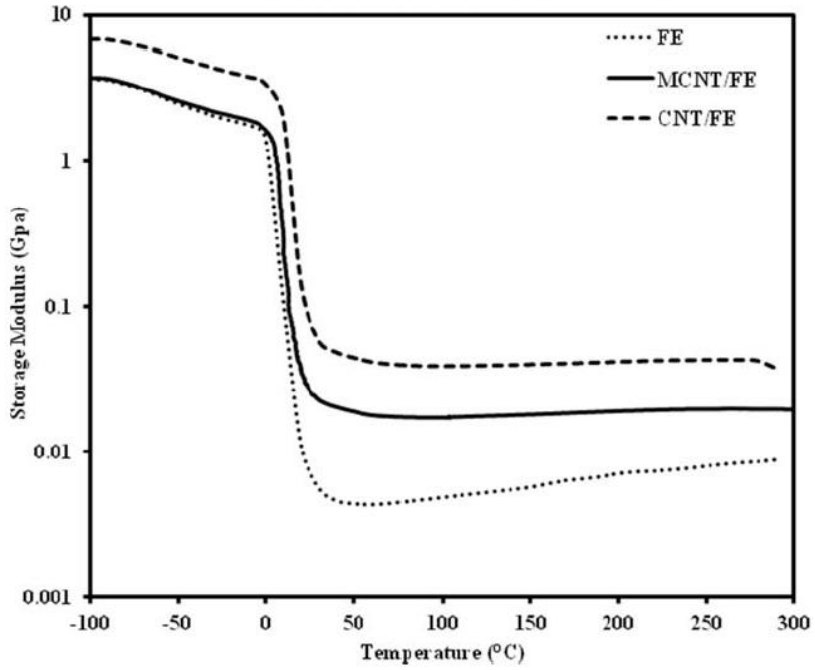

Figure 22. Storage modulus—temperature curves (DMA) for Viton® and Viton®/filler. FE, MCNT, and CNT are fluoroelastomer Viton®, modified carbon nanotube, and carbon nanotube, respectively (reproduced with permission from Wiley).[104]

These authors[105] also tested CNT- and CB-filled Viton® and unfilled Viton® for heat air aging. The tensile properties of Viton® were improved before and after heat aging with CNT addition. Independent of whether the samples were filled, a stress-induced crystallization occurred during tension, yielding crystals in γ-form. While for both matured and un-matured probes, the level of crystallinity was small, the un-aged probes' crystallinity level enhanced tremendously upon tensile stretching. Elongation break had the following increasing order: Viton®/CNT< Viton®/CB<unfilled Viton®, while that of tensile strength was: unfilled Viton®< Viton®/CB< Viton®/CNT.

Liu et al.[106] reported the morphological, rheological, and mechanical characteristics of Viton® GF-200S/multi-walled nanotube (MWNT) composites by an open two-roll mill followed by vulcanization within a compression-molding process. Viton®/MWNT composites displayed a higher level of cross-linking and better mechanical tendencies than those of Viton®/CB. Inserting 5 wt% MWNT in the Viton®

matrix improved the hardness, the tensile strength, and the abrasion resistance of Viton® by 12, 120, and 13%, respectively. MWNTs indicated greater reinforcing effectiveness than CB, and surface area yielded greater cross-link level and polymer-filler interaction.

As mentioned above, one of the major tested properties of THV is its rheological characteristics.[107-108] Lakshminarayanan et al.[107] studied the influence of clay surfactant and clay fraction on the rheology and morphology of untreated THV/clay nanocomposites obtained by blending from the melt. Furthermore, the same team utilized DyneonTM® FPO 3741 (a THV grade with 69.5 % fluorine content) and various grades of untreated and organo-modified Cloisite® NA, 15A, 20A, 30B, and 93A. The major motivating factor was that blending in the melt to obtain rubber/clay nanocomposites has the benefit of exploiting classical rubber mixing equipment and techniques. In clay-based polymer composite materials, the nano-filler dispersion shapes the final properties. These authors[107] also mixed clays in three different loadings, viz. 2.5, 5.0, and 10.0 phr and noted that, as the clay fraction increased, G' also increased (Figure 23).

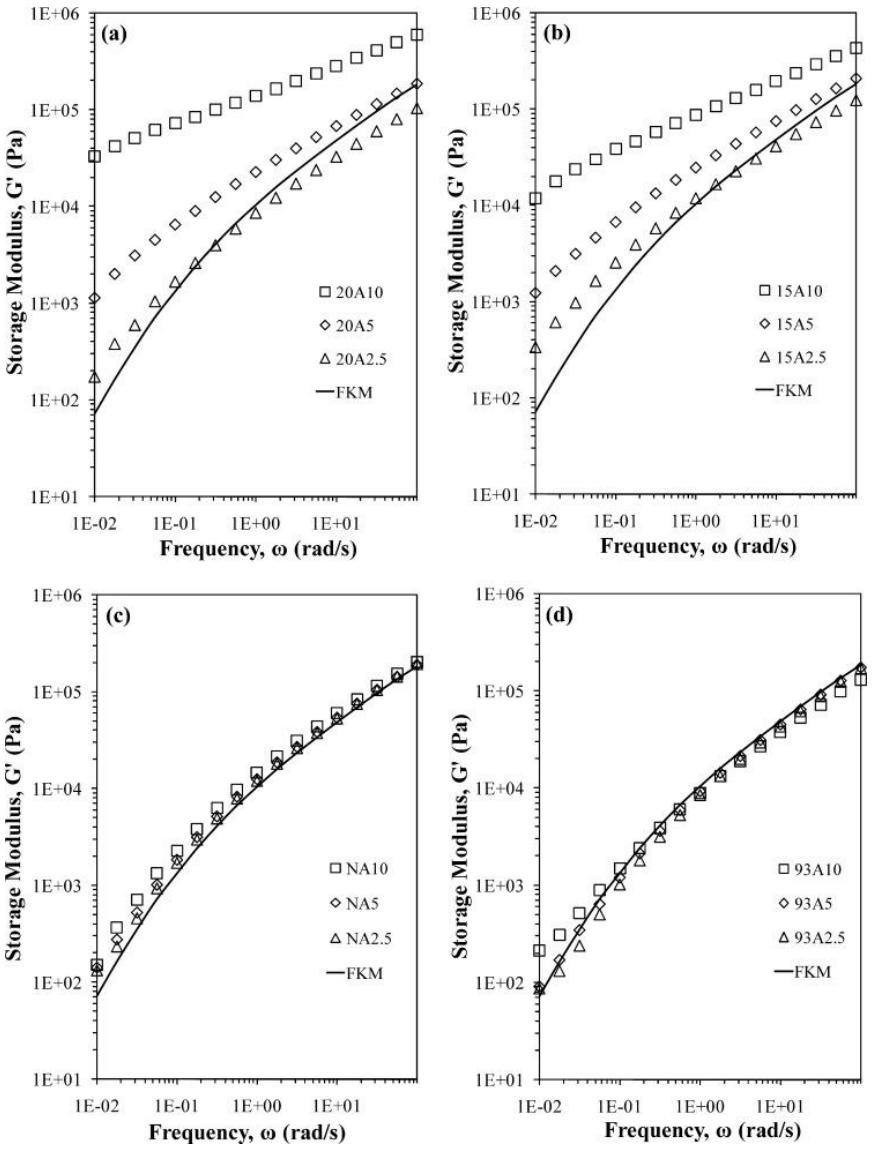

Figure 23. Storage moduli (G') measured at various frequencies at 180 ^{o}C for filled and unfilled THV composites with different concentrations (a) Cloisite® 20A, (b) Cloisite® 15A, (c) Cloisite® NA, and (d) Cloisite® 93A.[107] Clays were utilized at three distinct loading levels: 2.5, 5.0, and 10.0 phr (reproduced with permission from Wiley).

At high filler additions, the reliance of G' on frequency decreased and yielded a lower slope in the low-frequency region, attributed to a change over from a liquid-like to a solid-like behavior.[109-110] The utilization of organo-modified nano-clays results in drops of the G' beneath that of the polymer at greater frequencies without revealing the

precise mechanism. Cloisite® 20A and 15A allowed more dispersed THV composite materials to exhibit solid-like attitudes and stronger reinforcing influence, in contrast to the literature findings that reported a better dispersion of natural nanoclay in THVs.[98] XRD patterns revealed that nanoclays 20A yielded a *d*-spacing of 3.27 nm, indicating that THV molecules could insert the silicate galleries of these nanoclays. The rheological study confirmed the intercalation of 20A and 15A. In the composites of THV with 20A and 15A, the modulus increased approximately linearly with enlarging clay filling, proposing the existence of intercalation even at greater clay fillings. High magnification TEM results proved polymer molecules' dispersion and intercalation of clay layers (Figure 24).

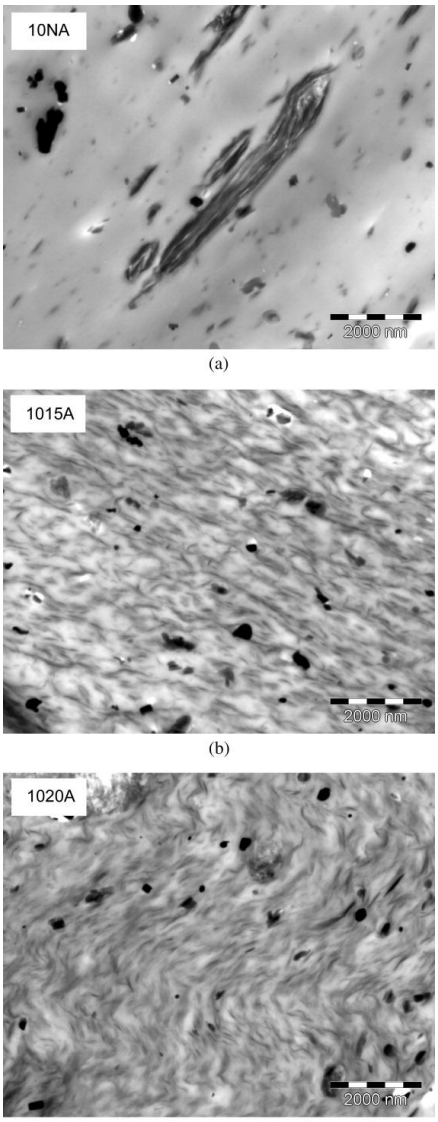

Figure 24. TEM images of THV/clay nanocomposites. 10NA, 1015A, 1020A stand for THV / clay CloisiteNA, THV / clay Cloisite15A, and THV / clay Cloisite20A, respectively.[108] Clays were utilized loading levels of 10.0 phr (reproduced with permission from Wiley).

The same authors[108] also focused on vulcanization and mechanical characteristics of nanocomposites based on a THV (Dyneon® FPO 3741) and 10 phr MMT. Unmodified (Cloisite NA) and di(hydrogenated tallow-alkyl) dimethyl ammonium modified (Cloisite 15A and Cloisite 20A) were utilized. The properties of THV and MMT-based nanocomposites were compared to those of composites prepared by 10 and

30 phr of CB. The influence of MMT concentration on the vulcanization behavior, the mechanical and dynamical tendencies of peroxide-treated composites were explored. Upon the vulcanization step, deintercalation of the clays and a decrease in *d*-spacing were revealed by XRD measurements. The organoclays slowed down the THV peroxide vulcanization process. Higher maximum torque on vulcanization was observed with the nanocomposites based on THV and organoclays compared to those prepared by THV and unmodified clay or THV and CB. The morphologies of organoclay/THV nanocomposites demonstrated similar intercalated/exfoliated structures. The highest increase in properties of THV/clay nanocomposites, such as torque and modulus, was observed in the organoclay with the lowest surfactant concentration (95 meq/100 g clay). The organoclays could enlarge the hydrodynamic strengthening and hysteresis loss of THV/clay nanocomposites. Uncured THV/clay composites were obtained utilizing the experimental protocol of the previous report.[107] Then, the nanocomposites were formulated by adding ZnO (3 phr), TAlC (3 phr), and peroxide (3 phr) and continued blending for 15 minutes only to ensure cross-linking. For changes induced by vulcanization, such as de-intercalation, the authors suggested two primary reasons: i) the interference of organic intercalants in the curing reaction[111] and ii) the influence of treating pressure.[112] In intercalated nanocomposites, a small percentage of THV trapped into the nanoclay matrices behaved like a filler, giving an increased operative volume percentage of the filler and enhancing hydrodynamic reinforcement in the matrix. Clay intercalation and exfoliation provided more rigidity to the Dyneon® FPO 3741 elastomer matrix.

4. Lessons Learned and Future Perspectives

Tables 5 and 6 give the molar percentages of the co-monomers in the THV samples. Among all THV grades, HFP units have the lowest percentage, excluding THV-A, THV-B, and THV-C studied by Zhang et al.[113] because HFP is not able to homopolymerize and thus less reactive than TFE and VDF.[55] Molar percentages of HFP in the THV grades were low ranging between 10.4%[67] and 26.7%.[62] Several studies investigated THV probes with close molar percentages of the three monomers.[9, 78, 85, 90,

[92] THV 500 was reported by Emmons et al.,[13] while H-THV was studied by Möller et al.,[90] and THV 500 investigated by Siengchin et al.[92] (Table 5), and THV 500G, tested by Duchesne et al.[114], have approximately the same percentages for the three monomers. From a future perspective, it can be suggested that new THV samples with different comonomer ratios could be synthesized for possible improvements for different applications. For instance, the TFE monomer could be lowered, with a higher VDF fraction to process the terpolymer easily, to lower the T_g value, and/or dissolve in common organic solvents. Hence, novel THV with high crystallinity picturing similarity to VDF rather than TFE could be derived. Such a THV sample with high crystallinity, as in VDF, might also have applications in piezoelectric materials. The insertion of HFP in other TFE terpolymers, such as poly(TFE-*ter*-HFP-*ter*-PVE)[21] and poly(TFE-*ter*-HFP-*ter*-AA),[23] might influence the properties. Varying the HFP fraction could reveal the potential influence of the HFP and $–CF_3$ groups on the characteristics of some TFE terpolymers.

Analysis of the sequence orders revealed that THV is an unsystematic terpolymer with a lower alternating fraction, such as VDF-TFE, TFE-HFP, including two or three TFE units next to each other. This sequence order and the HFP units lower the crystallinity of THV, which arises mainly from TFE units. Obviously, VDF units lower the T_m of THV grades compared to that of PTFE. The sequence orders of THV could be distributed on the topmost layer of thin films, as revealed by XPS, so that surface energy is lowered with higher water contact angles.[73] In utilizing TFE-based terpolymers at solid interphases, the wettability of TFE terpolymers needs to be considered.

Table 5. Co-monomer molar percentages of different THV grades studied in the literature.

Sample Name As Named in Reference	**Mole Percentages TFE /HFP/VDF**	**Reference**
THV	39.0/11.0/50.0	[9]
THV	39.0/11.0/50.0	[78]

Sample L (L: Linear)	10.0/18.0/72.0	[74]
FLS 2690	19.0/23.0/58.0	[61]
FT2481	17.0/20.0/63.0	[61]
Terpolymer A	22.8/26.7/50.5	[62]
Terpolymer B	20.9/18.0/61.1	[62]
THV 221G	51.4/10.4/38.2	[67]
THV terpolymer A	10.8/22.4/66.8	[69]
THV terpolymer B	24.2/23.0/52.8	[69]
THV 500	56.0/12.0/32.0	[13]
THV	36.0/12.0/52.0	[85]
FKM	14.9/19.9/65.2	[87]
L-THV	39.0/11.0/50.0	[90]
H-THV	56.0/12.0/32.0	[90]
THV 220	40.0/10.0/50.0	[92]
THV 500	55.5/12.0/32.5	[92]
THV 500G	56.0/12.0/32.0	[114]
THV	21.3/19.0/59.7	[115]
THV-200	42.0/20.0/38.0	[116]
THV-400	53.0/18.0/29.0	[116]

Table 7 gives the molar percentages and different modified TFE terpolymers studied in the literature.

Table 6. Co-monomer weight percentages of different THV grades studied in the literature.

Sample Name As Named in Reference	**Weight Percentages TFE /HFP/VDF**	**Reference**
THV-A	59.0/22.0/19.0	[113]

THV-B	67.5/17.5/15.0	[113]
THV-C	76.0/13.0/11.0	[113]
THV220	48.5/18.5/35.7	[117]
THV500	59.0/19.0/22.0	[117]
THV815	76.1/10.9/13.0	[117]
THV-15	67.5/17.5/15.0	[118]
THV-11	76.0/13.0/11.0	[118]
THV 500G	59/19/22	[114]

Table 7. Co-monomer molar percentages of different modified TFE terpolymers studied in the literature.

Sample Name As Named in Reference	**Molar Percentages**	**Reference**
TFE-(OR)-CH-CH_2-CH-CH_2- | O-CH_2-CH_2-X	45-55/35-54.8/0.2-10.0	[17]
TFE-(CF_3NO)-($CN_3O_2CCFClNO$)	50/40/10	[18]
TFE-P-VDF	48-38/49-29/3-33	[29]
TFE-P-GVE	50-60/40-50/0.01-10	[22]
TFE-P-TFP	59.5/37.3/3.2	[31]
TFE-P-VDF	39.3/24.3/36.4	[31]
TFE-VAc-PDMSMA	40.4-67.6/57.4-13.0/2.2-19.3	[26]
TFE-HFP-AA	95.2-88.3/0.4-3.7/4.4-8.0	[23]
TFE-HFP-AAc (THA-1)	94.7/0.2/5.1	[39]
TFE-HFP-AAc (THA-2)	88.5/0.7/10.8	[39]
TFE-P-NBVE	49.34-38.52/49.64-19.84/1.02-41.64	[30]
TFE-E-HFP	53.2-47.7/44.1-43.8/2.7-8.5	[32]
TFE-E-NFH	53.6-52.6/45.6-44.9/0.8-2.5	[32]
TFE-E-NFH	53.6-58.1/45.7-38.6/0.8-3.3	[33]
TFE-E-HFP	53.5-53.4/43.8-42.0/2.7-4.6	[33]
TFE-P-VDF	40/25/35	[119]

Wettability relies on the scale of the intermolecular interactions between contacting liquids and solids, and it is a valuable characteristic of natural or industry-generated materials for potential applications.[120-121] Superhydrophobic surfaces with

water contact angles above 150° have gained scientific and industrial interest. For example, recent studies on THV indicate that the surface could be treated to increase contact angle by various approaches, such as the non-solvent method.[67, 73] The industrial applications of superhydrophobic coatings require further efforts before finding possible applications of TFE terpolymers with contact angles as high as 140° in different areas such as self-cleaning surfaces. The concerned reader could reference Erbil's perspective report comprehensively focused on wettability-related issues.[120] Tuning surfaces of the TFE terpolymers might also result in non-adhesive materials resembling the climbing talent of creatures such as ants and geckos.[122]

An essential issue in synthesizing TFE-based terpolymers is the use of environmentally friendly solvents. Environmental concerns force academic and industry researchers to use non-toxic and green solvents and produce suitable fluoroelastomers.[123] Among the potential solvents, such as sc CO_2, water is the greenest solvent for synthesizing high molar mass-PTFE (reaching several million g/mol).[124] Therefore, researchers must consider this important aspect in developing novel TFE-based terpolymers. As suggested, the synthesis of TFE-based terpolymers with sc CO_2 could be an emerging area. Moreover, recently established synthetic methods, such as controlled radical polymerization,[125] will be widely exploited in future studies, potentially by combining with other more established polymerization technologies, and fluorinated low surface energy polymers will have a significant role in biomaterials science, electronics, and fuel cell membranes.[126]

The approach of Muñoz et al.[127], defined as teaching new tricks to old polymers, was applied to synthesize a semi-fluorinated poly(aryl ethers). The same methodology of interfacial polymerization could be utilized to improve the crystallinity of TFE-based terpolymers. The synthetic chemistry on cyclic perfluoropolyether[128] could be extended to TFE-based terpolymers to synthesize new fluorinated terpolymers.

All these recent examples indicate the importance of TFE-based FPs, the uniqueness of which makes them irreplaceable materials.[129] Moreover, most of them are bio-inert, safe, and durable, in contrast to some low molar-mass per and poly-fluoroalkyl substances (PFASs), well-established to be water soluble, and thus mobile, also toxic, persistent, bio-accumulative.[130] Fluoroelastomers are insoluble in water and thus not

mobile. Since FPs do not display the same characteristics as those of low molar mass-PFASs and are not involved in *quasi* same applications, they must be separated from the PFAS family (which gathers more than 12,000 compounds).[129] The PFASs are currently undergoing severe attacks (especially in media, EU, and EPA, which aim at restricting or even banning them). Interestingly, these high-performance polymers satisfy the 13 PLC criteria[4] in their recommended conditions of use. Their production is quite low, with 330,300 tons of FPs in 2021, compared to the yearly global production of plastics (> 460 million tons the same year). Furthermore, more recent innovative manufacturing (such as involving non-fluorinated surfactants in emulsion (co)polymerization of fluoro-olefins and improvements of releasing less and less fluorinated gases and waters) by most chemical producers of FPs have been announced.[131] This review also shows that these specialty polymers with unique properties are essential for our daily lives (electronics, internet of things, energy, transportation, etc.). So far, they are irreplaceable since suggested alternative materials, such as hydrocarbon polymers used in similar conditions, fail.[132] They also represent a special family apart from other "conventional" C1-C10 PFASs found everywhere on Earth and in the oceans. In the future, recycling (e.g., the unzipping depolymerization of FKM or FKKM), end-of-life of F-elastomers, their risk assessment, and their circular economy must be considered.[133-134]

The interested reader could benefit from the recent Howe's report on the potential ^{19}F NMR measurements on FPs.[135] The improvements in spectroscopic methods will ease the detailed characterization of modified TFE terpolymers. Besides, the increasing accessibility of low-field benchtop ^{19}F NMR with high-temperature capabilities might help to investigate the dynamics of modified TFE terpolymers in bulk and confined geometry.

Another important subclass of TFE terpolymers contains phosphorus.[136] For example, they perform better in i) anticorrosion coatings due to the strong adhesion ability of the phosphonic acid onto the surfaces of metals, ii) recovering rare earth elements or heavy metals, and as flame-retardants,[136] and iii) satisfying the increasing need to generate materials for self-cleaning applications. Depending on the use of functional groups in synthesizing such terpolymers, the conductivity of TFE terpolymers might be enhanced, leading to novel applications in fuel cell membranes.[36-37] In

particular, expanding the family of TFE terpolymers with phosphorus should interest both industrial and academic researchers.

TFE terpolymers, either unmodified or modified as clay-based composites prepared from solution or in melt containing MMT, clay, and CNT, have been well studied.[35, 96, 98-99, 103-105] In the pure state, *d*-spacing in crystalline domains could be related to the microstructures of THV. The widening in *d*-spacing was explained by the insertion of particular quantities of the HFP units into the THV 221G crystals.[137] In THV/clay composites, Cloisite® nanoclays 20A yielded a *d*-spacing of 3.27 nm, evidencing the insertion of THV molecules in the silicate galleries of these nanoclays and the affinity of 20A nanoclay towards THV.[98] Similarly, an increase in the *d*-spacing of the clay mineral-packed fluoroelastomer indicated the establishment of the intercalated silicate layer.[35, 100]

To enhance various properties, the TFE terpolymers were cured. The terpolymers based on TFE, PMVE, and CNVE, where CNVE is CF_2=CFOCF_2CF(CF_3)OCF_2CF_2CN[138] were reacted with a fluorinated diazido crosslink agent under Huisgen "click chemistry".[139] Other strategies was applied to poly(TFE-*ter*-PMVE-*ter*-VDF), poly(TFE-*ter*-PMVE-*ter*-E), poly(TFE-*ter*-P-*ter*-VDF) fluoroelastomers by cure-site monomers bearing nitrile, alkyne, [51] or azido groups. [138-139]

Moreover, surface modification on TFE-based terpolymers could reveal these materials' antimicrobial behavior.[140] In addition, the bactericidal mechanism of thin films of TFE-based terpolymers could also be an important scientific target. Surface modification of TFE-based terpolymers could result in soft elastomeric and non-tacky materials, or the lower surface energy C-F bonds could yield non-sticky arrangements.[141]

5. Conclusions

In conclusion, exploring alternative FPs, particularly TFE-based terpolymers, has demonstrated promising advancements in overcoming the challenges of i) decomposition at elevated temperatures closer to melting temperature and ii) insoluble in common

organic solvents associated with PTFE processing. Moreover, the crystallinity of the alternative PFs could also be tuned by using various groups, such as CF_3 in HFP. These unique and excellent properties of TFE fluoropolymers make them an alternative to PTFE and irreplaceable.

Contrarily to concerns surrounding certain PFAS, TFE-based terpolymers have shown resilience in meeting performance requirements while avoiding the adverse environmental impact often associated with specific PFAS. By embracing a commitment to responsible material usage and environmental stewardship, we can ensure that ongoing research and development efforts prioritize the enhancement of polymer properties and the long-term sustainability of these materials. Through the integration of eco-friendly practices (as well as hydrocarbon and/or bio-sourced surfactants in copolymerization of TFE with other fluoro-olefins) and the promotion of awareness regarding the compatibility of irreplaceable TFE-based terpolymers, which preserve their outstanding properties in aggressive media in a wide range of temperatures and mechanical stress, polymer scientists can chart a course toward a more sustainable and technologically advanced future. Moreover, advancements in characterization methods help with investigating TFE-based terpolymers at solid interphases in thin films and under various conditions, including confinement and high pressures.

There are still open question marks remaining on various aspects of TFE-based terpolymers, including synthesis, surface modification, and correlating the microstructures of TFE-based terpolymers to their properties. Could we develop proper methods for the recovery of waste of TFE-based terpolymers?[142] Could we utilize TFE terpolymers for new applications, such as special coatings in fabricated textiles, new medical devices, polymer composites as viscosity reducers, or sand consolidation material in the petroleum industry and items related to ecologic transitions? How may we anticipate the recycling of such fluoropolymers containing various reactants as fillers (plasticizers, antistatic, colorizing dyes, and other additives)? How do novel TFE polymers anticipate the PFAS restriction? How could TFE-based terpolymers change their morphology and hydrophobicity in thin films or under confinement in nanoporous proxies at solid interphases by solvent and/or non-solvent vapor annealing? The

anticipated answers to these questions and the relevant findings could be participated by the researchers of the academy and the industry in the current decade.

Conflicts of interest

The authors declare that they have no known competing financial interests or personal relationships that could have appeared to influence the work reported in this paper.

Acknowledgments

The authors thank all coworkers cited in the references below and sponsors for Research including CNRS.

References.

[1] R. J. Plunket (Kinetic Chemicals, Inc.), *U.S. Patent 2230654*, **1941**.

[2] D. J. Boday, in *Advances in Fluorine-Containing Polymers ACS Symposium Series*, (Eds: D. W. Smith, S. T. Iacono, D. J. Boday, S. C. Kettwick), American Chemical Society, Washington, DC, USA 2012, Ch. 1.

[3] S. Ebnesajjad, In *Plastics Design Library, Applied Plastics Engineering Handbook,* Second Edition (Ed: M. Kutz) William Andrew Publishing, Oxford, UK 2017, Ch. 4.

[4] S. H. Korzeniowski, R. C. Buck, R. M. Newkold, A. E. Kassmi, E. Laganis, Y. Matsuoka, B. Dinelli, S. Beauchet, F. Adamsky, K. Weilandt, V. K. Soni, D. Kapoor, P. Gunasekar, M. Malvasi, G. Brinati, S. Musio, *Integr. Environ. Assess. Manag.* **2023**, 19, 326.

[5] H. Teng, *Appl. Sci.* **2012**, *2*, 496.

[6] *Fluorinated Polymers: Volume 1: Synthesis, Properties, Processing and Simulation,* (Eds: B., Améduri, H., Sawada) Royal Society of Chemistry, Cambridge, UK **2017**.

[7] B. Ameduri. *Chem. Rev.* **2009**, *109*, 6632.

[8] B. Ameduri. *Macromol. Chem. Phys.* **2020**, *221*, 1900573.

[9] D. Auhl, J. Kaschta, H. Münsted, H. Kaspar, K. Hintzer, *Macromolecules* **2006**, *39*, 2316.

[10] D. W. Grainger, in *Biomaterials Science*, Fourth Edition (Eds: W. R. Wagner, S. E. Sakiyama-Elbert, G. Zhang, M. J. Yaszemski), Academic Press, London, UK 2020, Ch. 1.3.2C.

[11] J. Lv, Y. Cheng, *Chem. Soc. Rev.* **2021**, *50*, 5435.

[12] Y. Roina, F.; Auber, D. Hocquet, G. Herlem, *Materials, Today Chem*., **2021**, 20, 100412.

[13] E. D. Emmons, N. Velisavijevic, J. R. Schoonover, D. M. Dattelbaum, *Appl. Spectrosc.* **2008**, *62*, 142.

[14] J. Scheirs, in *Modern Fluoropolymers*, (Ed: J. Scheirs), John Wiley and Sons, Chichester, UK 1997, Ch. 1.

[15] D. A. Hercules, C. A. Parrish, J. S. Thrasher, in *Fluorinated Polymers: Volume 2: Applications.* (Eds: B. Ameduri, H. Sawada), Royal Society of Chemistry, Cambridge, England 2017, Ch. 9.

[16] S. Selman, E. N. Squire (E. I. du Pont de Nemours and Company), *U.S. Patent 3308107*, **1967**.

[17] D. B. Pattison (E. I. du Pont de Nemours and Company), *U.S. Patent 3306879*, **1967**.

[18] W. H. Oliver, E. C. Stump (Calgon Corporation), *U.S. Patent 3472822*, **1969**.

[19] J. F. Harris (E. I. du Pont de Nemours and Company), *U.S. Patent 3449304*, **1969**.

[20] R. J. Jones (TRW Inc.), *U.S. Patent 3761453*, **1973**.

[21] D. P. Carlson (E. I. du Pont de Nemours and Company), *U.S. Patent 4029868*, **1977**.

[22] T. Eguchi (Individual), *U.S. Patent 4321306*, **1982**.

[23] G. K. Kostov, A. N. Atanasov, *J. Appl. Polym. Sci.* **1991**, *42*, 1607.

[24] B. Ameduri, B. Boutevin, G. Kostov, P. Petrov, P. Petrova, *J. Polym. Sci.: Part A: Polym. Chem.* **1999**, *37*, 3991.

[25] B. Baradie, M. S. Shoichet, *Macromolecules* **2002**, *35*, 3569.

[26] B. Baradie, M. S. Shoichet, *Macromolecules* **2005**, *38*, 5560.

[27] A. E. Feiring, M. K. Crawford, W. B. Farnham, J. Feldman, R. H. French, K. W. Leffew, V. A. Petrov, F. L. Schadt III, R. C. Wheland, F. C. Zumsteg, *J. Fluor. Chem.* **2003**, *122*, 11.

[28] J. Shifmann, D. G. Shell (Dayco Products, Inc.), *U.S. Patent 6365250*, **2002**.

[29] K. Yamamoto, J. Asakura, T. Miwa, M. Saito, *J. Fluor. Chem.* **2004**, *125*, 735.

[30] G. K. Kostov, O. Matsuda, Y. Tabata, S. Machi, *J. Polym. Sci.: Part A: Polym. Chem.* **1992**, *30*, 1077.

[31] W. W. Schmiegel, *KGK Kautschuk Gummi Kunststoffe* **2004**, *57*, 313.

[32] K. Arai, A. Funaki, S. Phongtamrung, K. Tashiro, *Polymer* **2009**, *50*, 4612.

[33] A. Funaki, S. Phongtamrug, K. Tashiro, *Polym. J.* **2013**, *45*, 545.

[34] C. A. Parrish, *Ph.D. Thesis*, Clemson University **2017**.

[35] M. A. Kader, C. Nah, *Polymer* **2004**, *45*, 2237.

[36] M. Yamabe, K. Akiyama, Y. Akatsuka, M. Kato, *Eur. Polym. J.* **2000**, *36*, 1035.

[37] S. V. Kotov, S. D. Pedersen, W. Qiu, Z. M. Qiu, D. I. Burton, *J. Fluorine Chem.* **1997**, *82*, 13.

[38] E. K. Gladding, R. Sullivan (E. I. du Pont de Nemours and Company), *U.S. Patent 3546186*, **1970**.

[39] G. K. Kostov, A. N. Atanassov, *Eur. Polym. J.* **1991**, *27*, 1331.

[40] G. Kostov, B. Ameduri, B. Boutevin, G. Bauduin, M. Stankova, *J. Polym. Sci.: Polym. Chem.* **2004**, *42*, 1693.

[41] J. W. Jacks (Acadia Polymers), *U.S. Patent 5753718*, **1998**.

[42] K. Hintzer, F. D. Jochum, H. Kaspar, K. H. Lochhaas, T. C. Zipplies (3M), *WO Patent 2015/134435 A1*, **2015**.

[43] K. Hintzer, F. D. Jochum, H. Kaspar, K. H. Lochhaas, T. C. Zipplies (3M), *WO Pat. 2015/088784 A2*, **2015**.

[44] D. E. Hull, B. V. Johnson, I. P. Rodricks, J. B. Staley, in *Modern Fluoropolymers*, (Ed: J. Scheirs), John Wiley and Sons, Chichester, England **1997**, Ch. 13.

[45] E. B. Twum, *Ph.D. Thesis*, University of Akron **2013**.

[46] V. Arcella, R. Ferro, in *Modern Fluoropolymers*, (Ed: J. Scheirs), John Wiley and Sons, Chichester, England **1997**, Ch. 2.

[47] P. Bonardelli, G. Moggi, A. Turturro, *Polymer* **1986**, *27*, 905.

[48] J. A. Hiltz, *J. Anal. Appl. Pyrolysis* **2014**, *109*, 283.

[49] M. Pianca, P. Bonardelli, M. Tato, G. Cirillo, G. Moggi, *Polymer* **1987**, *28*, 224.

[50] B. Ameduri, Fluoroelastomers: Current Status and Future Applications. Encyclopedia of Polymer Science and Technology, 2023, DOI: 10.1002/0471440264.pst137.pub2

[51] A. Taguet, B. Ameduri, B. Boutevin, *Adv. Polym. Sci.* **2005**, *184*, 127.

[52] D. Li, M. Liao, *J. Fluor. Chem.* **2017**, *201*, 55.

[53] S. Huber, M. K. Moe, N. Schmidbauer, G. H. Hansen, D. Herzke, Emissions from Incineration of Fluoropolymer Materials, Norwegian Institute for Air Research, Norway, **2009**.

[54] R. E. Uschold, *Polym. J.* **1985**, *17*, 253.

[55] W. W. Schmiegel, *Macromol. Chem.* **1979**, *76*, 39.

[56] E. B. Twum, E. F. McCord, D. F. Lyons, P. A. Fox, P. L. Rinaldi, *Eur. Polym. J.* **2014**, *51*, 136.

[57] P. C. Painter, M. M. Coleman, *Fundamentals of Polymer Science*, Technomic Publishing Co. Inc., Lancaster, USA **1994**.

[58] G. Odian, *Principles of Polymerization, 4th ed.*; Wiley-Interscience, New Jersey,

USA **2004**.

[59] H. Kaspar, K. Hintzer, T. Zipplies, R. Kaulbach (3M), WO 2004/094491A1, **2004**.

[60] Y. M. Murasheva, A. S. Shashkov, A. A. Dontsov, *Polymer Science U.S.S.R.* **1981**, *23*, 711.

[61] S. F. Dec, R. A. Wind, G. E. Maciel, *Macromolecules*, **1987**, *20*, 2754.

[62] P. K. Isbester, J. L. Brandt, T. A. Kestner, E. J. Munson, *Macromolecules*, **1998**, *31*, 8192.

[63] S. Ok, *Ph.D. Thesis*, Technical University of Dresden **2008**.

[64] M. F. Kemmere, in *Supercritical Carbon Dioxide in Polymer Reaction Engineering,* (Eds: M. F. Kemmere, T. Meyer), Wiley-VCH, Weinheim, Germany, **2005**, Ch. 1.

[65] R. Sui, A. S. Rizkella, T. J. Charpentier, *Langmuir* **2005**, *21*, 6150.

[66] M. A. McHugh, C. A. Mertdogan, T. P. Dinoia, C. Anolick, W. H. Tuminello, R. Wheland, *Macromolecules* **1998**, *31*, 2252.

[67] S. Ok, S. Sadaf, L. Walder, *High Perform. Polym.* **2014**, *26*, 779.

[68] E. B. Twum, E. F. McCord, D. F. Lyons, P. L. Rinaldi, *Macromolecules* **2015**, *48*, 3563.

[69] S. Ok, *Magn. Reson. Chem.* **2015**, *53*, 130.

[70] E. Mavroudakis, D. Cuccato, M. Dossi, G. Comino, D. Moscatelli, *J. Phys. Chem. A* **2014**, *118*, 238.

[71] L. Li, E. B. Twum, X. Li, E. F. McCord, P. A. Fox, D. F. Lyons, P. L. Rinaldi, *Macromolecules* **2012**, *45*, 9682.

[72] E. B. Twum, E. F. McCord, P. A. Fox, D. F. Lyons, P. L. Rinaldi, *Macromolecules* **2013**, *46*, 4892.

[73] S. Ok, J. Sheets, S. Welch, S. Kaya, A. Jalilov, D. R. Cole, *J. Polym. Sci. Part B: Polym. Phys.* **2017**, *55*, 643.

[74] P. Maccone, M. Apostolo, G. Ajroldi, *Macromolecules*, **2000**, *33*, 1656.

[75] V. Arcella, G. Brinati, M. Apostolo, *Chim. Ind.* **1997**, *79*, 345.

[76] V. Arcella, G. Brinati, M. Albano, V. Tortelli (Ausimont S.p.A.), *U.S. Patent 5585449*, **1996**.

[77] V. Arcella, G. Brinati, M. Albano, V. Tortelli (Ausimont S.p.A.), *U.S. Patent 5612419*, **1997**.

[78] A. Ram, J. Miltz, *J. Appl. Polym. Sci.* **1971**, *15*, 2639.

[79] J. Stange, S. Wächter, H. Münster, H. Kaspar, *Macromolecules* **2007**, *40*, 2409.

[80] A. M. Dessouki, N. H. Taher, M. El-Arnaouty, F. H. Khalil, *J. Appl. Polym. Sci.* **1993**, *48*, 1249.

[81] A. M. Dessouki, N. H. Taher, M. B. El-Arnaouty, *Polym. Int.* **1999**, *48*, 92.

[82] U. Lappan, U. Geissler, U. Gohs, *Macromol. Mater. Eng.* **2011**, *296*, 843.

[83] A. Funaki, K. Arai, S. Aida, S. Phongtamrug, K. Tashiro, *Polymer* **2008**, *49*, 5497.

[84] The Society of the Plastics Industry. The Guide to the Safe Handling of Fluoropolymer Resins-Fifth Edition BP-101, Washington, USA **2019**.

[85] H. Freimuth, C. Sinn, M. Dettenmaier, *Polymer* **1996**, *37*, 831.

[86] G. Moggi, P. Bonardelli, J. C. Bart, *Polym. Bull.* **1982**, *7*, 115.

[87] B. D. Kaushiva, G. L. Wilkes, C. Comeaux, L. Socha, *Polymer* **2001**, *42*, 4619.

[88] A. L. Logothetis, *Prog. Polym. Sci.* **1989**, *14*, 251.

[89] L. F. Pelosi, A. L. Moran, A. E. Burroughs, T. L. Pugh, *Rubber Chem. Technol.* **1976**, *49*, 367.

[90] D. Möller, H. Münstedt, H. Kaspar, *Rheol. Acta* **2009**, *48*, 509.

[91] H. Kaspar, K. Hintzer, *Rheol. Acta* **2011**, *50*, 577.

[92] S. Siengchin, T. N. Abraham, *J. Appl. Polym. Sci.* **2012**, *127*, 919.

[93] P. Rost, E. Horemans, in *Automotive Fuel Containment*, Rapra Technology Limited, Birmingham, **2000**, Paper 6.

[94] S. Khanra, A. Kumar, D. Ganguly, S. K. Ghorai, S. Chattopadhyay, *J. Polym. Res.* **2022**, *29*, 174.

[95] D. Feldman, *J. Macromol. Sci. Part A* **2005**, *42*, 587.

[96] M. A. Kader, M. Y. Lyu, C. Nah, *Compos. Sci. Technol.* **2006**, *66*, 1431.

[97] M. Maiti, A. K. Bhowmick, *J. Appl. Polym. Sci.* **2006**, *101*, 2407.

[98] M. Maiti, A. K. Bhowmick, *Polym. Eng. Sci.* **2007**, *47*, 1777.

[99] M. Maiti, A. K. Bhowmick, *J. Appl. Polym. Sci.* **2007**, *105*, 435.

[100] A. D. Mali, N. G. Shimpi, S. Mishra, *Polym. Int.* **2014**, *63*, 338.

[101] N. G. Shimpi, A. D. Mali, S. Mishra, *Polym. Bull.* **2016**, *73*, 3033.

[102] H. A. Zen, A. B. Lugao, *RevistaMateria* **2017**, *22*, e-11845.

[103] J. Heidarian, A. Hassan, *Composites: Part B* **2014**, *58*, 166.

[104] J. Heidarian, A. Hassan, *Polym. Comp.* **2016**, *37*, 3341.

[105] J. Heidarian, A. Hassan, *Pol. J. Chem. Tech.* **2016**, *19*, 132.

[106] Y. Liu, P. Liu, Z. Fan, H. M. Duong, *Mater. Tech.: Adv. Func. Mater.* **2015**, *30*, 150.

[107] S. Lakshminarayanan, B. Lin, G. A. Gelves, U. Sundararaj, *J. Appl. Polym. Sci.* **2009**, *112*, 3597.

[108] S. Lakshminarayanan, G. A. Gelves, U. Sundararaj, *J. Appl. Polym. Sci.* **2012**, *124*, 5056.

[109] R. Valsecchi, M. Vigano, M. Levi, S. Turri, *J. Appl. Polym. Sci.* **2006**, *102*, 4484.

[110] W. S. Chow, Z. A. M. Ishak, J. Karger-Kocsis, *J. Macromol. Mater. Eng.* **2005**, *290*, 122.

[111] K. G. Gatos, J. Karger-Kocsis, *Polymer* **2005**, *46*, 3069.

[112] Y. R. Liang, Y. L. Lu, Y. P. Wu, Y. Ma, L. Q. Zhang, *Macromol. Rapid Commun.* **2005**, *26*, 926.

[113] S. Zhang, C. Zou, D. I. Kushner, X. Zhou, R. J. Orchard, N. Zhang, Q. M. Zhang, *IEEE Trans. Electr. Insul.* **2012**, *19*, 1158.

[114] D. Duchesne, H. Kaspar, L. P. Chen, K. Hintzer, A. Molnar, L. Mayer, G. Löhr (Dyneon LLC), *U.S. Patent No. 6489420*, **2002**.

[115] H. Hori, H. Tanaka, T. Tsuge, R. Honma, S. Banerjee, B. Ameduri, *Euro. Polym. J.* **2017**, *94*, 322.

[116] T. Fukushi (Minnesota Mining and Manufacturing Company), *U.S. Patent 5827587*, **1998**.

[117] C. Li, G. Chen, X. Qiu, M. Gao, R. Gerhard, *Appl. Phys. Lett.* **2020**, *13*, 011003.

[118] K. W. Yi, J. Liu, Y. Zhou, X. P. Hu, S. H. Zhang, B. J. Chu, *Sci. China Phys. Mech. Ast.* **2020**, *63*, 227721.

[119] A. Ghosh, R. S. Rajeev, A. K. Bhattacharya, A. K. Bhowmick, S. K. De, *Rubber Chem. Technol.* **2003**, *76*, 220.

[120] Y. Erbil, *Langmuir* **2020**, *36*, 2493.

[121] M. Wolfs, T. Darmanin, F. Guittard, *Polym. Rev.* **2013**, *53*, 460.

[122] K. Autumn, A. M. Peattie, *Integr. Comp. Biol.* **2002**, *42*, 1081.

[123] Y. Wang, Y. Bai, X. Zheng, *Polym. Intern.* **2019**, *68*, 1952.

[124] G. J. Puts, P. Crouse, B. M. Ameduri, *Chem. Rev.* **2019**, *119*, 1763.

[125] G. Puts, V. Venner, B. Ameduri, P. Crouse, *Macromolecules* **2018**, *51*, 6724.

[126] H. Peng, *Polym. Rev.* **2019**, *59*, 739.

[127] G. Muñoz, K. M. Chamberlain, S. Athukorale, G. Ma, X. Gu, C. U. Pittman, D. W. Smith, *Macromol. Rapid Comm.* **2023**, *44*, e2200737.

[128] S. Honda, N. Ikuta, M. Oka, S. Yamaguchi, S. Handa, *Macromol. Rapid Comm.* **2022**, *43*, 2100567.

[129] B. Ameduri, *Molecules* **2023**, *28*, 7564.

[130] B. Ameduri, *Perfluoroalkyl substances: Regulations, synthesis and applicationg Applications*, Royal Society of Chemistry, Oxford, **2022**.

[131] B. Ameduri, J. Sales, M. Schlipf, ITRC *Intern. Chem. Regul. Law Rev.* **2023**, *6*, 18.

[132] P. C. Sherrell, A. Šutka, M. Timusk, A. Šutka, *Small* **2024**, 2311570 (DOI: 10.1002/smll.202311570).

[133] B. Ameduri, H. Hori, *Chem. Soc. Rev.* **2023**, *52*, 4208.

[134] J. Schuster, J. Lutz, Y. P. Shaik, V. R. Yadavalli, *Adv. Indust. Engin. Polym. Res.* **2022**, *5*, 248.

[135] P. W. A. Howe, *Prog. Nuc. Magn. Reson. Spec.* **2020**, *118-119*, 1.

[136] M. Wehbi, A. Mehdi, C. Negrell, G. David, A. Alaaeddine, B. Ameduri, *ACS Appl. Mater. Interfaces* **2020**, *12*, 1, 38.

[137] S. Ok, B. Hartmann, H. Duran, H. Eickmeier, M. Haase, U. Scheler, M. Steinhart, *J. Polym. Sci., Part B: Polym. Phys.* **2019**, *57*, 1402.

[138] M.-H. Hung, B. Ameduri, B. Boutevin, G. Tillet (E. I. du Pont de Nemours and CNRS), US2013/012673 *B2*.

[139] G. Tillet, G. Lopez, M.-H. Hung, B. Ameduri, *J. Polym. Sc. Part A Polym. Chem.*, **2015**, 53, 1171–1173

[140] M. Haktaniyan, M. Bradley, *Chem. Soc. Rev.* **2022**, *51*, 8584.

[141] J. Cuthbert, M. R. Martinez, M. Sun, J. Flum, L. Li, M. Olszewski, Z. Wang, T. Kowalewski, K. Matyjaszewski, *Macromol. Rapid Commun.* **2019**, *40*, e1800876.

[142] A. Lakshmanan, S. K. Chakraborty, in *Sintering Techniques of Materials*, (Ed: A. Lakshmanan) InTechOpen, **2015**, Ch. 9.